

Density profiles in the raise and peel model with and without a wall; physics and combinatorics

Francisco C Alcaraz¹, Pavel Pyatov² and Vladimir Rittenberg³

¹ Instituto de Física de São Carlos, Universidade de São Paulo, Caixa Postal 369, 13560-590, São Carlos, SP, Brazil

² Bogoliubov Laboratory of Theoretical Physics, JINR 141980 Dubna, Moscow Region, Russia

³ Physikalisches Institut, Universität Bonn, Nussallee 12, 53115 Bonn, Germany
E-mail: alcaraz@if.sc.usp.br, pyatov@theor.jinr.ru and vladimir@th.physik.uni-bonn.de

Received 12 October 2007

Accepted 11 December 2007

Published 4 January 2008

Online at stacks.iop.org/JSTAT/2008/P01006

[doi:10.1088/1742-5468/2008/01/P01006](https://doi.org/10.1088/1742-5468/2008/01/P01006)

Abstract. We consider the raise and peel model of a one-dimensional fluctuating interface in the presence of an attractive wall. The model can also describe a pair annihilation process in disordered unquenched media with a source at one end of the system. For the stationary states, several density profiles are studied using Monte Carlo simulations. We point out a deep connection between some profiles seen in the presence of the wall and in its absence. Our results are discussed in the context of conformal invariance ($c = 0$ theory). We discover some unexpected values for the critical exponents, which are obtained using combinatorial methods. We have solved known (Pascal's hexagon) and new (split-hexagon) bilinear recurrence relations. The solutions of these equations are interesting in their own right since they give information on certain classes of alternating sign matrices.

Keywords: algebraic structures of integrable models, exact results, stationary states

ArXiv ePrint: [0709.4575](https://arxiv.org/abs/0709.4575)

Contents

1. Introduction	2
2. Raise and peel models with and without a wall	5
3. Some exact results and some conjectures	9
4. Density profiles in the raise and peel models with and without a wall in the stationary states	12
5. The raise and peel model with and without a wall in continuous time. Temperley–Lieb algebras	20
6. Hexagon recurrence relations	22
6.1. Pascal’s hexagon	23
6.2. Split hexagon	24
7. Combinatorics in the stationary states of the RPM	25
8. Clusters in the stationary states of the RPMW and RPM	27
8.1. Case of L odd	28
8.2. Case of L even	29
9. Conclusions	32
Acknowledgments	33
Appendix. The RPM as a pair annihilation process with a source	33
References	37

1. Introduction

The raise and peel model (RPM) is discussed in several papers [1, 2] (for a review see [3]). This is a one-parameter dependent stochastic model of a one-dimensional fluctuating interface. The RPM can be seen as a model for wetting in which the adsorption is local (the interface raises) and the desorption is non-local (the interface is peeled). The parameter is given by the ratio of the adsorption and desorption rates. When the two rates are equal (the Razumov–Stroganov point) the Hamiltonian which describes the time evolution of the system is conformally invariant and the stationary states have remarkable combinatorial properties. The origin of these properties can be traced back to the definition of the model in terms of generators of the Temperley–Lieb (TL) algebra at the semigroup point. This algebra has two representations which are relevant for us: one in terms of link patterns (which makes the connection with the interface model) and another one in terms of an integrable XXZ quantum chain with L sites (which allows one to obtain the spectrum of the Hamiltonian and its conformal properties).

The fluctuating interface is described by RSOS (Dyck) paths which can be interpreted as clusters of tiles deposited on a substrate. The heights at both ends of the system vanish. The clusters touch each other at contact points. In [4], a conjecture for the average number

of clusters at the Razumov–Stroganov point in the stationary states was given. According to this conjecture, the average size of a cluster increases like $L^{1/3}$ (L is the size of the system, L even). In the present paper we give combinatorial arguments in favor of this conjecture. We also show that the average size of the cluster at one of the ends of the system also increases like $L^{1/3}$. This is in contrast to a model in which the RSOS paths are taken with equal probabilities when one obtains $L^{1/2}$.

An interesting result obtained in [2] using Monte Carlo simulations is the behavior of the density of contact points in the finite-size scaling limit. It has the functional form expected from conformal invariance for a one-point function with an unexpected exponent. Further details on this observation will be given in the next sections.

In the present paper we extend the RPM at the Razumov–Stroganov point in two ways. Firstly we consider the case when the size of the system L is an odd number. This implies a change of the configuration space of the model, one has ballot paths with fixed ends: one at height 1 the other one at height zero. We call them one-step Dyck paths. The model is still based on the TL algebra at the semigroup point. We also consider the RPM in the presence of a wall (RPMW). The model is based on the one-boundary TL algebra [5, 6] at the semigroup point. The configuration space is now given by ballot paths [7] with one end fixed at zero and the other one free, corresponding to the wall. In the bulk the rules for adsorption and desorption as in the original RPM but at the wall one has a new adsorption process with an arbitrary fixed rate a (for convenience the bulk rates are taken equal to one).

For both extensions conformal invariance is obeyed and the stationary states have new combinatorial properties.

There is an alternative interpretation [8] of the RPMW. One can see the stochastic process as a pair annihilation process in unquenched disordered media (see the appendix for detailed explanations). In this description, one has clusters of tiles which either touch each other or are separated by impurities (defects). There are no empty sites. The defects can either hop over a cluster peeling its surface or they can annihilate in pairs if the defects are on neighboring sites. The clusters change in shape and number like in the usual RPM. The rates of all these processes are fixed at the value one. At one end of the system one has a source of defects which acts with a rate a . The source acts as follows: if a cluster touches the end of the system, a layer of the cluster is desorbed and a defect is added at each of the two ends of the peeled cluster. In the stationary states, the average number of defects corresponds to the average height of the ballot paths at the wall.

In the ‘defects’ interpretation of the model, the RPM for L odd can be seen as a system in which one impurity (defect) hops at large distances in unquenched disordered media. During the hop, the media are changed (the cluster over which the defects hops, is peeled).

This paper has two distinctive parts: a physical one and a mathematical one. Physics is in the first part of the paper (sections 2–4), mathematics is concentrated in the second part. The two parts can be read independently.

In section 2 we present the stochastic models describing the RPM models with or without a wall. This presentation is suitable for Monte Carlo simulations. We also define some relevant observables. The alternative description of the model in terms of defects is given in the appendix.

In section 3 we present without proof some exact results for the stationary states obtained in the last part of the paper. We give the expressions for the average number of clusters for any size of the system. In particular we give the large L behavior. These expressions are relevant because they are the integrated quantities of the density of contact points, the latter being obtained from Monte Carlo simulations. In particular we derive the values of the critical exponents.

We show a surprising identity between the probability density function (PDF) to have the first cluster at distance x from the wall for the RPMW and the PDF to have defect at distance x from the boundary for the RPM for an odd number of sites. As shown in section 4 this PDF has remarkable properties in the finite-size scaling limit.

We also give some conjectures for the average values of the number of sites where adsorption can take place. From their values one can derive the average number of tiles desorbed (desorption takes place through avalanches [2]).

In section 4 we present the results obtained from Monte Carlo simulations. Firstly we remind the reader about the observation [2] that in the stationary state of the RPM (L even) the density of contact points, in the finite-size scaling limit is given by the expression expected from conformal invariance with an exponent $1/3$ while we should expect an exponent $2/3$ (the one-point function of an operator with conformal spin vanishes).

We next consider the presence of the wall in the model with a boundary rate a and study the density of contact points profile in the finite-size scaling limit. It is independent of the boundary rate a and has a functional form suggested by conformal invariance with the same exponent $1/3$ as in the absence of the wall.

We also study the density of defects profile and find that in the finite-size scaling limit it has the functional dependence expected from conformal invariance with (again!) an unexpected exponent.

In the finite-size scaling limit, the probability distribution function to have a cluster at distance x/L from the wall stays, surprisingly, a probability density function (its integrated value is equal to one) and is independent of a i.e. is universal. The functional dependence of this PDF is similar to what is expected from conformal invariance for a one-point function. No explanation for this observation was found.

In section 5 we present the derivation of the RPM and RPMW in continuum time using the Temperley–Lieb algebra [9] and its one-boundary extension [5] at the semigroup points and make the connection with the spin-half XXZ quantum chain. Based on this connection and the integrability of the chain, one can show that our systems are conformally invariant. This section is a review of known results.

In section 6 we present firstly the bilinear recurrence relations called the Pascal's hexagon. The relations are not new but the solutions, specified by the boundary conditions are. We next propose some new bilinear relations that we called the split-hexagon relations and give their solutions for certain boundary conditions. This section is pure mathematics.

In sections 7 and 8 we make the contact with physics and derive the results enumerated in section 3. Firstly in section 7, for the RPM we derive the probabilities to have k clusters for a system of size L (L even and odd).

In section 8 we consider the RPMW. For L odd we show a remarkable connection between the RPMW and the RPM for the same value of L . In particular one can show that independently of a value of the boundary rate a all properties of clusters, except the first, are identical. The case of the RPMW with L even and arbitrary values of a is more

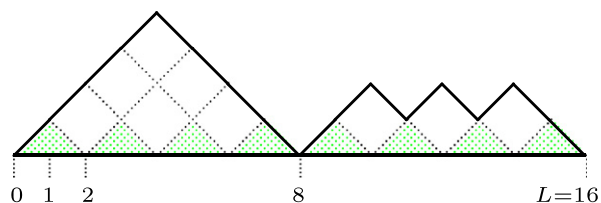


Figure 1. A configuration of the interface given by a Dyck path with three contact points and two clusters for a lattice size $L = 16$. The size of the leftmost cluster is equal to 8. The substrate is also shown (the dashed region).

subtle. Nevertheless for the case $a = 1$ we were able to derive the probability of having k clusters in a system of size L .

Our conclusions are presented in section 9.

2. Raise and peel models with and without a wall

We consider a one-dimensional lattice with $(L + 1)$ sites. An interface is formed by attaching at each site non-negative integer heights h_i which obey the restricted solid-on-solid (RSOS) rules:

$$h_{i+1} - h_i = \pm 1, \quad h_i \geq 0, \quad i = 0, 1, \dots, L. \quad (2.1)$$

We will consider three kind of interfaces, each with different configuration spaces depending on the conditions at the boundaries (the values of h_0 and h_L):

(i) Dyck path configurations.

One takes L even and $h_0 = h_L = 0$. There are

$$C_L = \frac{L!}{(L/2)!(L/2 + 1)!} \quad (2.2)$$

configurations of this kind. An example of such a configuration for $L = 16$ is shown in figure 1.

To characterize the interface, it is useful to define several quantities. A *contact point* is a site j where $h_j = 0$. A *cluster* is the domain between two consecutive contact points. The *size* of the leftmost cluster is j , if $j \neq 0$ is the smallest number for which $h_j = 0$.

It is useful to visualize the interface as a film of tiles (tilted squares) deposited on a *substrate* defined by the Dyck path $h_i = (1 - (-1)^i)/2$ ($i = 0, 1, \dots, L$). In this picture the clusters can be seen as droplets of a fluid deposited on the substrate.

(ii) One-step Dyck paths configurations.

One takes L odd, $h_0 = 1$ and $h_L = 0$. There are C_{L+1} configurations of this kind. An example of such a configuration for $L = 15$ is shown in figure 2.

The one-step Dyck paths can be mapped onto configurations with clusters and one defect (impurity). In order to obtain these configurations one draws a horizontal line at height one through the first (leftmost) cluster starting at $h_0 = 1$. If the first cluster has size x ($h_x = 0$), the horizontal line intersects the cluster at $(x - 1)$. One puts a defect at the point $(x - 1/2)$ and one lowers the cluster by one unit:

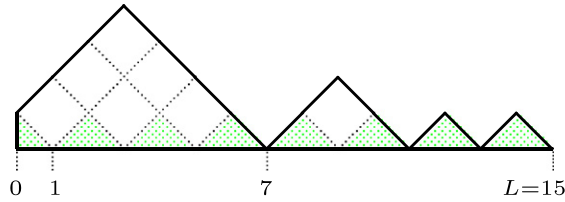


Figure 2. A one-step Dyck path configuration with four contact points and four clusters for $L = 15$. The leftmost cluster has size 7.

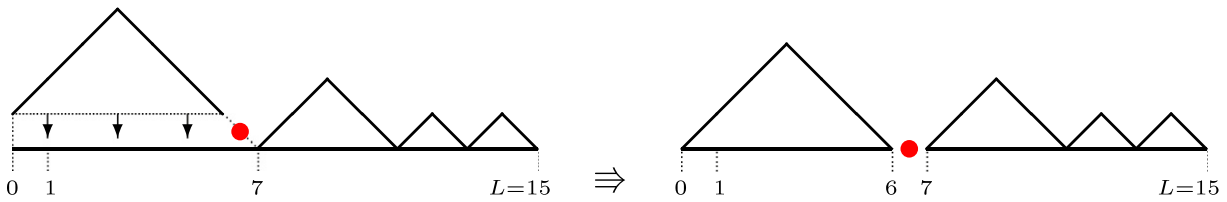


Figure 3. Mapping the one-step Dyck path shown in figure 2 onto a configuration with one defect and clusters.

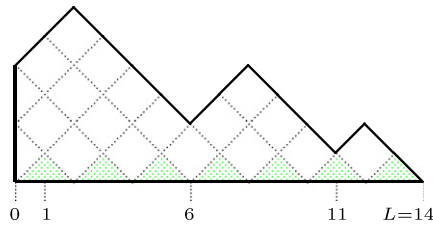


Figure 4. A ballot path for $L = 14$. One has one contact point and one cluster of size 14.

$h_j \rightarrow (h_j - 1) \forall j = 0, 1, \dots, x - 1$. This procedure is illustrated in figure 3 for the configuration shown in figure 2.

(iii) Ballot paths.

One takes (for both L even and odd) $h_L = 0$ and h_0 free ($h_0 = L, L - 2, \dots, 0$ or 1).⁴ There are

$$\binom{L}{\lfloor L/2 \rfloor} \tag{2.3}$$

configurations of this kind (here $\lfloor n \rfloor$ is the integer part of n). An example of such a configuration for $L = 14$ is shown in figure 4.

The ballot paths configurations can be seen as droplets of a fluid in the presence of a wet wall.

Similar to the case of one-step Dyck paths, one can map the ballot paths onto configurations with clusters and defects (impurities). We will call them configurations with defects. The mapping follows the same procedure as the one used for one-step Dyck paths and is illustrated in figure 5. Notice that the height at the origin h_0 is equal to the number of defects.

⁴ In the usual definition [7], a ballot path is defined by taking h_0 fixed.

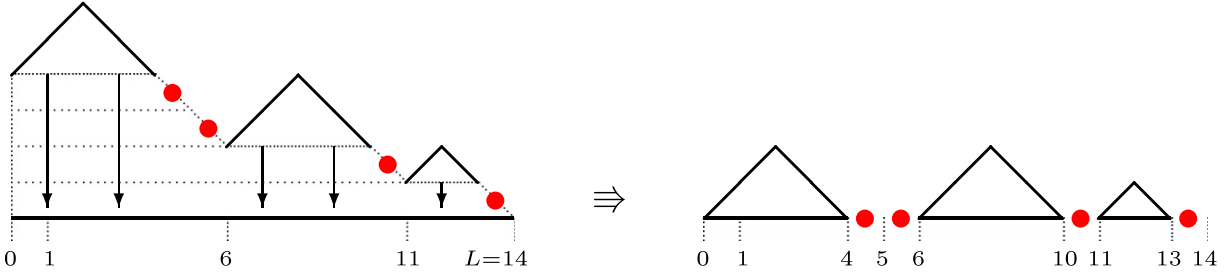


Figure 5. The mapping of the ballot path shown in figure 4 onto a configuration with four defects.

The configurations with defects can also be seen as an interface in which the droplets have empty spaces between them.

In the raise and peel model (RPM) the dynamics of the interface is described in a transparent way in the language of tiles (tilted squares) which cover the area between the interface and the substrate. We consider the interface separating a film of tiles deposited on the substrate from a rarefied gas of tiles. The interface can be Dyck path, one-step Dyck path or ballot path configurations (the dynamics for defect configurations is discussed in the appendix).

The evolution of the system in discrete time (Monte Carlo steps) is given by the following rules. With a probability $P_i = 1/(L-1)$ a tile from the gas hits the site $i, i = 1, \dots, L-1$. Depending on the value of the slope $s_i = (h_{i+1} - h_{i-1})/2$ at the site i , the following processes can occur:

- (i) $s_i = 0$ and $h_i > h_{i-1}$.
The tile hits a local peak and is reflected.
- (ii) $s_i = 0$ and $h_i < h_{i-1}$.
The tile hits a local minimum. With a probability 1 the tile is adsorbed ($h_i \mapsto h_i + 2$).
- (iii) $s_i = 1$.
With probability 1 the tile is reflected after triggering the desorption of a layer of tiles from the segment ($h_j > h_i = h_{i+b}, j = i+1, \dots, i+b-1$), i.e. $h_j \mapsto h_j - 2$ for $j = i+1, \dots, i+b-1$. This layer contains $b-1$ tiles (this is always an odd number). For an example see figure 6.
- (iv) $s_i = -1$.
With probability 1 the tile is reflected after triggering the desorption of a layer of tiles belonging to the segment ($h_j > h_i = h_{i-b}, j = i-b+1, \dots, i-1$), i.e. $h_j \mapsto h_j - 2$ for $j = i-b+1, \dots, i-1$.

Notice that the adsorption and desorption rates were taken equal, this is the RPM at the Razumov–Stroganov point. The model was studied in detail in the case of Dyck path configurations (L even) also when the adsorption and desorption rates are different and the phase diagram of the model was obtained (see [1, 2], for a review see [3]). The Razumov–Stroganov point is special in two ways. Firstly, the Hamiltonian which gives the continuous time evolution of the system can be mapped into an XXZ spin-half quantum

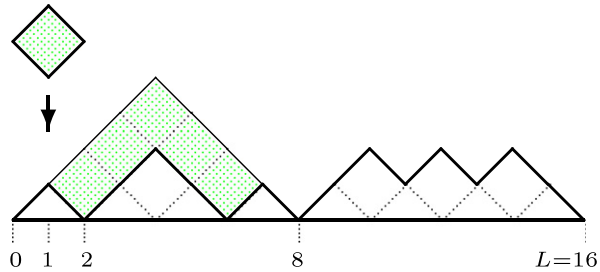


Figure 6. A desorption event. The incoming tile at site 1 triggers an avalanche of 5 tiles, which are shaded. All the shaded tiles are removed in the desorption event.

chain which is integrable [10]. The finite-size scaling limit of the Hamiltonian spectrum is given by $c = 0$ Virasoro characters (c is the central charge of the Virasoro algebra) and hence the system is conformally invariant. Secondly, the probability distribution function (PDF) describing the stationary state of the system for finite systems has remarkable combinatorial properties [11, 12] which allows one to obtain exact results for physical observables.

The RPM was also considered in the L odd case and it was shown that the defect (see figure 3) makes Lévy flights and behaves like a ‘relativistic’ random walker (dispersion relation $\langle x^2 \rangle \sim t^2$) [8]. In the present paper we are going to present more results which will show some surprising properties of this model.

The PDF describing the stationary states is expressed in terms of Dyck paths only. The dynamics seen in the space of defect configurations is interesting: it describes the pair annihilation of two defects in unquenched random media. The average density of defects decreases like $1/t$ [8].

We are going to extend the RPM model acting on ballot paths by making the first site active (site 0 in figures 4 and 5). We will define in this way the RPM in the presence of a wall (RPMW).

The evolution of the system (Monte Carlo steps) is given by the following rules. With a probability $P_i = 1/(L + a - 1)$ a tile from the gas hits the site $i, i = 1, \dots, L - 1$. The changes of the interface produced by the hits are the same as in the RPM model. With a probability $P_0 = a/(L + a - 1)$, a half-tile hits the site 0. The boundary rate is equal to a , as opposed to the bulk rates which are equal to 1. If the slope $s_0 = h_1 - h_0$ is equal to 1, the half-tile gets adsorbed (see figure 7). If $s_0 = -1$, the half-tile is reflected. Notice that the adsorption process is local. This is not the case if one uses the defect configurations picture (see the appendix).

The RPMW in its time continuous version, can be obtained in a simple way using a Hamiltonian expressed in terms of generators of the one-boundary Temperley–Lieb algebra. This is explained in section 5. Similar to the RPM model, the stationary states of the RPMW have magical combinatorial properties for finite values of L [13]–[15]. New expressions and relations are summarized in section 3 and derived in sections 7 and 8. Moreover, the Hamiltonian can be mapped onto an integrable XXZ spin-half quantum chain and the finite-size scaling limit of the Hamiltonian spectrum is known [16]. It can be expressed in terms of Virasoro characters therefore, similar to the RPM, the

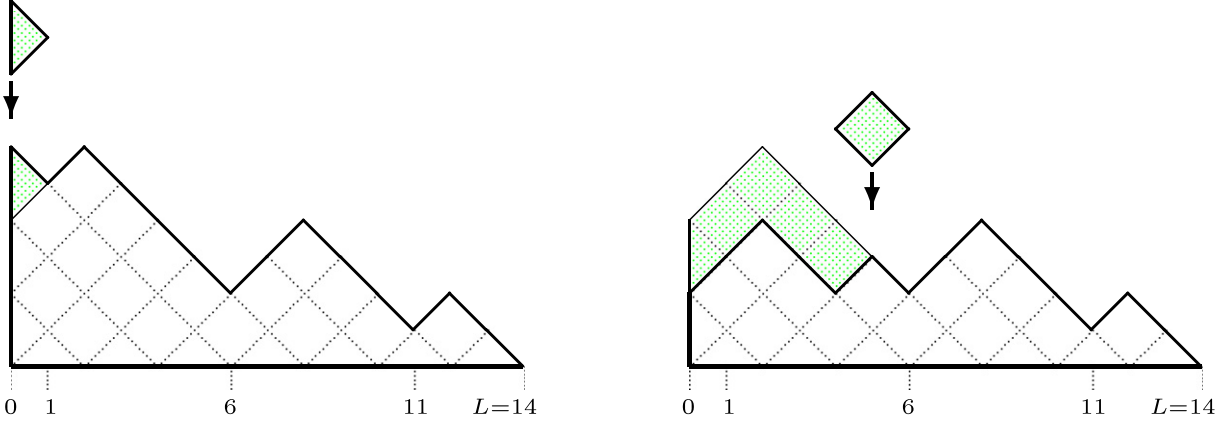


Figure 7. The adsorption of a half-tile at the first site and desorption of a layer touching the boundary for the ballot path shown in figure 4.

RPMW is conformally invariant. The consequences of this observation will be presented in section 4.

3. Some exact results and some conjectures

In this section we present some exact results which will be discussed in sections 7 and 8. These results, besides being interesting in their own right, will be used in section 4 to derive critical exponents and to check the data obtained in Monte Carlo simulations. We consider the RPM with and without a wall at the Razumov–Stroganov point and the boundary rate a .

We first introduce two useful functions $S(L, n)$ and $P(L, n, m)$. They are defined as follows:

$$S(L, n) = 2^{-\lfloor n^2/4 \rfloor} \prod_{p=1}^n \frac{1}{(2p-1)!!} \prod_{p=0}^{\lfloor (n-1)/3 \rfloor} \frac{(L - \lfloor (n+p)/2 \rfloor - p - 1)!}{(L - 2n + 3p)!} \times \prod_{p=0}^{\lfloor (n-2)/3 \rfloor} \frac{(2L + 2n - 6p - 3)!!}{(2L - 2\lfloor (n+p)/2 \rfloor + 4p + 1)!!}, \quad (3.1)$$

$$P(L, n, m) = 2^{\lfloor (m-1)/2 \rfloor} S(L, n-1) \frac{(2n-m)!(n-1)!}{m!(n-m)!(2n-1)!} \times \frac{(L-2n+m-1)!(L-n)!(2L-2n+2m-1)!!}{(L-2n-1)!(L-n+\lfloor m/2 \rfloor)!(2L-2n+2\lfloor (m+1)/2 \rfloor-1)!!}. \quad (3.2)$$

The expressions (3.1) have first appeared in [13, 14]. The expressions for

$$S(L) = S(L, \lfloor (L-1)/2 \rfloor)$$

appear also in the problem of enumeration of vertically symmetric A_p^V and vertically and horizontally symmetric A_p^{VH} $p \times p$ alternating sign matrices (a known topic in

combinatorics [17]–[19]):

$$S(2N) = A_{2N+1}^V = \prod_{0 \leq i \leq N-1} \frac{(3i+2)(6i+3)!(2i+1)!}{(4i+2)!(4i+3)!}, \quad (3.3)$$

$$S(2N-1) = A_{4N-1}^{VH}/A_{2N-1}^V = A_{4N+1}^{VH}/A_{2N+1}^V = \prod_{0 \leq i \leq N-1} \frac{(3i+1)(6i)!(2i)!}{(4i)!(4i+1)!}. \quad (3.4)$$

We next fix the notation to be used below: for the RPMW of a size L and boundary rate a an observable $\Phi(\dots)$ is denoted as $\Phi_L^{(a)}(\dots)$. For the RPM of a size L the same function is denoted as $\Phi_L(\dots)$. Notice the obvious relation $\Phi_L^{(0)}(\dots) = \Phi_L(\dots)$.

We now state the following results for the stationary states of the RPM and RPMW.

In the RPM, the probability of having k clusters for a system of size L is:

$$P_L(k) = \frac{1}{S(L)} P\left(L, \left\lfloor \frac{L-1}{2} \right\rfloor, k-1\right). \quad (3.5)$$

For L even this result coincides with a conjecture made by de Gier [4].

In the presence of a wall (RPMW), the probabilities to have k clusters for a system of size L are:

$$\begin{array}{l} L \text{ odd,} \\ a \text{ arbitrary:} \end{array} \quad P_L^{(a)}(k) = P_L(k) = \frac{1}{S(L)} P\left(L, \frac{L-1}{2}, k-1\right), \quad (3.6)$$

$$\begin{array}{l} L \text{ even,} \\ a = 1 : \end{array} \quad P_L^{(1)}(k) = \frac{1}{S(L+1)} \left\{ P\left(L+1, \frac{L}{2}, k\right) + P\left(L+1, \frac{L}{2}-1, k-1\right) \right\}. \quad (3.7)$$

Note the remarkable fact that for L odd, the probabilities to have k clusters for the RPM with or without a wall are the same. This statement is valid for any value of a . Another connection between these two systems (with or without wall for L odd) will be presented below. The relation (3.7) for L even is valid only for $a = 1$.

Knowing the probabilities to find k clusters, one can compute the average number of clusters $\langle k \rangle_L$ and $\langle k \rangle_L^{(a)}$, for the RPM and RPMW, respectively. We give here only the large L limit behavior of these numbers:

$$\langle k \rangle_L \xrightarrow{L \rightarrow \infty} \begin{cases} \frac{\Gamma(1/3)\sqrt{3}}{2\pi} L^{2/3} \approx 0.738488 L^{2/3}, & (L \text{ even}) \\ \alpha L^{2/3}, & (L \text{ odd}) \end{cases} \quad (3.8)$$

$$\langle k \rangle_L^{(a)} \xrightarrow{L \rightarrow \infty} \alpha L^{2/3}, \quad (L \text{ even or odd, } a \text{ arbitrary}) \quad (3.9)$$

where approximants give for α the value $\alpha \approx 0.5056(3)$. Observe that in all cases the average size of a cluster increases like $L^{1/3}$. Notice that for the RPM for L even one has the largest number of clusters. The explanation is very simple. In the case L odd or in the presence of the wall, the first cluster near the active boundary has a size of the order of L (see the comment after equation (3.15)) which leaves less available space for the other clusters.

We now consider the probability densities $F_L^{(a)}(x)$ to have the leftmost (first) cluster end at a distance x from the wall for both L even and odd. These probability densities are

related to the probability density $D_L(x)$ to have the leftmost cluster end (which coincides with the position of the defect) at the point x for the RPM for L odd:

$$\begin{array}{l} L \text{ odd,} \\ a \text{ arbitrary:} \end{array} \quad F_L^{(a)}(x) = D_L(x), \quad x = 1, 3, \dots, L, \quad (3.10)$$

$$\begin{array}{l} L \text{ even,} \\ a = 1: \end{array} \quad F_L^{(1)}(x) = D_{L+1}(x+1), \quad x = 0, 2, \dots, L. \quad (3.11)$$

Moreover, the conditional probabilities to have the first cluster at distance x and any given configuration to the right of it are the same in the two models for any value of a if L is odd, and for $a = 1$ if L is even. In particular, the densities of the contact points (defined earlier and illustrated in figures 1, 2 and 4) at a distance x in the RPMW and in the RPM, $N_L^{(a)}(x)$ and $N_L(x)$, respectively, satisfy the relations

$$\begin{array}{l} L \text{ odd,} \\ a \text{ arbitrary:} \end{array} \quad N_L^{(a)}(x) = N_L(x), \quad x = 1, 3, \dots, L, \quad (3.12)$$

$$\begin{array}{l} L \text{ even,} \\ a = 1: \end{array} \quad N_L^{(1)}(x) = N_{L+1}(x+1), \quad x = 0, 2, \dots, L. \quad (3.13)$$

As discussed in the appendix, for L odd, in the RPM to a one-step Dyck path corresponds the one-defect picture in the configuration space. The probability density to have the defect at a distance x is obviously the same as at $(L-x)$, $x = \frac{1}{2}, \frac{5}{2}, \dots, (L - \frac{1}{2})$. This observation implies the following symmetry relations:

$$\begin{array}{l} L \text{ odd,} \\ a \text{ arbitrary:} \end{array} \quad F_L^{(a)}(x) = F_L^{(a)}(L+1-x), \quad x = 1, 3, \dots, L, \quad (3.14)$$

$$\begin{array}{l} L \text{ even,} \\ a = 1: \end{array} \quad F_L^{(1)}(x) = F_L^{(1)}(L-x), \quad x = 0, 2, \dots, L. \quad (3.15)$$

The symmetry relations (3.14) and (3.15) are surprising since one could expect that the probability density function should be biased towards the wall. Another important consequence is that the average size of the first cluster is $L/2$. This is in contrast with the RPM for L even when it is of order $L^{1/3}$ (see section 4).

Before closing this section we give a conjecture for the RPMW with the boundary rate $a = 1$. The fraction of the interface where adsorption can take place (this is the average number of local minima of the interface divided by L) is

$$A_L^{(1)} = \begin{cases} \frac{6L^2 + 8L - 5}{4(2L+1)(2L+3)}, & (L \text{ even}) \\ \frac{(6L^2 + 14L + 9)(L-1)}{4L(2L+1)(2L+3)}, & (L \text{ odd}). \end{cases} \quad (3.16)$$

These expressions were checked up to $L = 9$. It is amusing to note that simple guesses are possible for $A_L^{(1)}$. A similar situation occurred also for the RPM [1]. The expressions (3.16) will be used in section 4 to characterize the avalanches occurring in the model.

4. Density profiles in the raise and peel models with and without a wall in the stationary states

As mentioned in the previous sections, in the continuum limit, the RPM and the RPMW are conformally invariant and are described by a $c = 0$ conformal field theory [10, 16]. If the central charge of the Virasoro algebra vanishes, the scaling indices (highest weights of the irreducible representations of the Virasoro algebra) are:

$$\Delta_{p,q} = \frac{(3p - 2q)^2 - 1}{24}, \quad (4.1)$$

where p and q are non-negative integers. This implies that $\Delta_{p,q}$ is either an integer or it is equal to $1/3$ plus an integer.

A local operator ϕ is characterized by its scaling dimension X and conformal spin s :

$$X = \Delta_{p,q} + \bar{\Delta}_{p',q'}, \quad s = \Delta_{p,q} - \bar{\Delta}_{p',q'}. \quad (4.2)$$

If x is the distance from the origin (which coincides with i in the discrete versions described in section 2, $i = 0$ corresponds to $x = 0$) and L is the size of the system, in the scaling limit, one expects [20] the following density profile in the case of symmetric boundaries ‘ r ’:

$$\langle \phi(x/L) \rangle_{r,r} = \frac{C}{[L \sin(\pi x/L)]^X}, \quad (4.3)$$

where C is a constant.

The profile of a primary operator vanishes if its conformal spin is not zero [20] therefore one should have

$$X = 2\Delta_{p,q}. \quad (4.4)$$

The fact that one can make predictions for the functional dependence of the density profiles in stationary states is a consequence of the conformal invariance of the Hamiltonian which gives the time evolution of the stochastic process.

If the two boundaries are different ($r \neq s$), one expects [20]:

$$\langle \phi(x/L) \rangle_{r,s} = \frac{\Phi_{r,s}(\cos(\pi x/L))}{[L \sin(\pi x/L)]^X}, \quad (4.5)$$

where the function $\Phi_{r,s}$ is calculable.

Before discussing density profiles, it is instructive to have under our eyes typical profiles for finite lattices. For the RPM, L even, typical profiles are shown in [2]. In the case of the RPMW and finite L , the profiles depend on the boundary rate a . In figure 8 we show for $a = 1$, a typical configuration for $L = 128$. One notices that $h_0 = 4$ which implies that in the corresponding defect configuration one has four defects (see the appendix). One has a large leftmost cluster of size 124. In this paper we will not discuss the profile of the heights (for the RPM (L even) this was done in full detail in [2]) but we will show that the average height at the origin behaves like $\langle h_0 \rangle \sim \ln(L)$.

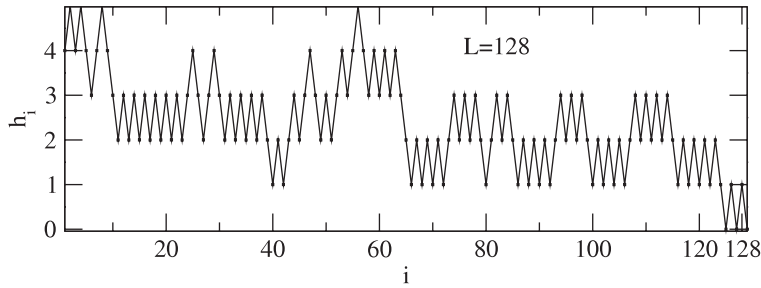


Figure 8. Typical configuration in the stationary state for the RPMW with a boundary rate $a = 1$. The system has a size $L = 128$. h_i is the height at site i .

We discuss several density profiles.

(1) *Density of contact points.*

(a) *The RPM model (L even). Density of contact points in Dyck path configurations.*

Since the average number of contact points is known (see (3.8)), if (4.3) is valid, we have to choose $X = 1/3$. The functional dependence of the density is therefore also fixed as well as the constant C in (4.3):

$$C = -\frac{\sqrt{3}}{6\pi^{5/6}} \Gamma\left(-\frac{1}{6}\right) \simeq 0.753\,149. \quad (4.6)$$

In order to check the prediction of conformal invariance, using Monte Carlo simulations on large lattices, we have measured the density of contact points $N_L(x)$. In figure 9 we show $N_L(x)[L \sin(\pi x/L)]^{1/3}/C$ for several lattice sizes. If the prediction (4.3) is correct, one should obtain the value 1 for this quantity. This is indeed the case. (Data with poorer statistics but indicating the same result were shown already in [2]).

One does not need to find the density of contact points for the RPM in the case L odd since it coincides (see section 3) with the one observed in the RPMW for a boundary rate $a = 1$ which is going to be discussed next.

(b) *The RPMW model. Density of contact points in ballot path configurations.*

In this case the boundary conditions at $x = 0$ and L do not coincide since for $x = 0$ one has the wall and for $x = L$, one has $h_L = 0$, fixed. For this reason one expects an expression like the one given by (4.5) [20] with the function $\Phi_{w,0}(\cos(\pi x/L))$ to be determined (here w corresponds to the wall, 0 corresponds to $h_L = 0$).

We start with the case in which the boundary rate is $a = 1$. Since the average number of clusters is known exactly (see (3.9)), the exponent X in (4.3) is $X = 1/3$. Monte Carlo simulations on large lattices suggest the following simple expressions for $\Phi_{w,0}(\cos(\pi x/L))$:

$$\Phi_{w,0} = \beta \left[1 - \cos\left(\frac{\pi x}{L}\right) \right]^{1/3}, \quad (4.7)$$

where

$$\beta = \sqrt{3}\alpha \simeq 0.8757(8). \quad (4.8)$$

This number is compatible with the data shown in figure 10.

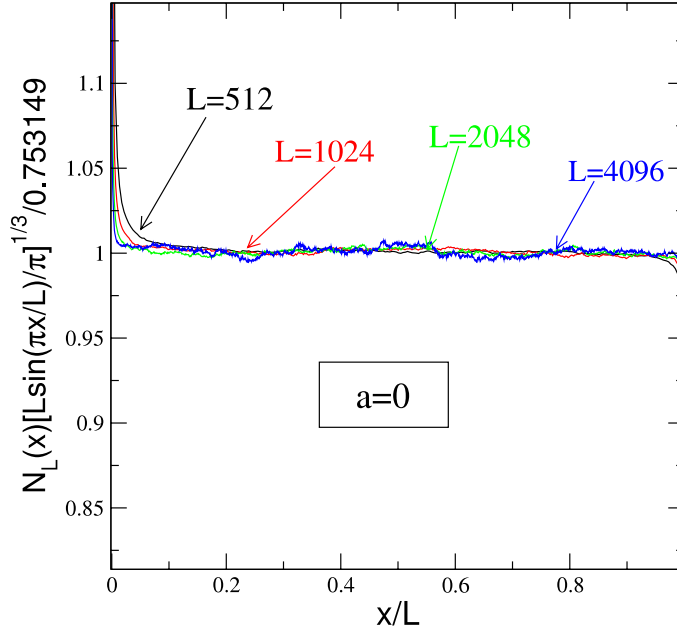


Figure 9. The RPM for L even. The density of contact points $N_L(x)$ multiplied by $[L \sin(\pi x/L)/\pi]^{1/3}/0.753149$ as a function of x/L for $L = 512, 1024, 2048$ and 4096 .

In order to make sure that the finite-size behavior of the density of contact points is indeed a consequence of conformal invariance, in figure 11, we give the density of contact points $N_L^{(a)}(x)$ multiplied by $[L \sin(\pi x/L)/(1 - \cos(\pi x/L))]^{1/3}$ for different boundary rates $a > 1$, and a fixed, large value of L . One notices that within errors the value of β in equation (4.7) stays unchanged. We repeated the study for $a < 1$ and for odd values of L . For L odd, as expected, we observe no a dependence of the density profiles.

It is known that the finite-size scaling limit of the Hamiltonian spectrum which gives the time evolution of the system is independent of the boundary rate a [16]. Consequently one could expect the space one-point function in the scaling limit to be also independent of a . This is indeed the case.

To sum up, the density of contact points in the presence of a wall, has for any boundary rate a and for both L even and odd, the expression:

$$N_L^{(a)}(x) \simeq 0.8757 \left[\frac{1 - \cos(\pi x/L)}{L \sin(\pi x/L)} \right]^{1/3}. \quad (4.9)$$

The same expression describes the density of contact points for the RPM (L odd) defined on one-step Dyck paths.

From (4.9) one learns that for small values of x (large L) one has very few clusters. This can be explained by the existence of a large leftmost cluster (see figure 8 and a quantitative argument below). At the other end of the system $x = L - y$, y small, the density of clusters is larger than in the Dyck path configurations (a factor of $0.8757 \times 2^{1/3} \simeq 1.103$ compared with 0.753).

Up to now we have not discussed the exponent $X = 1/3$ and we are going to see something unexpected. According to (4.4) one gets a scaling index $\Delta_{p,q} = 1/6$. This

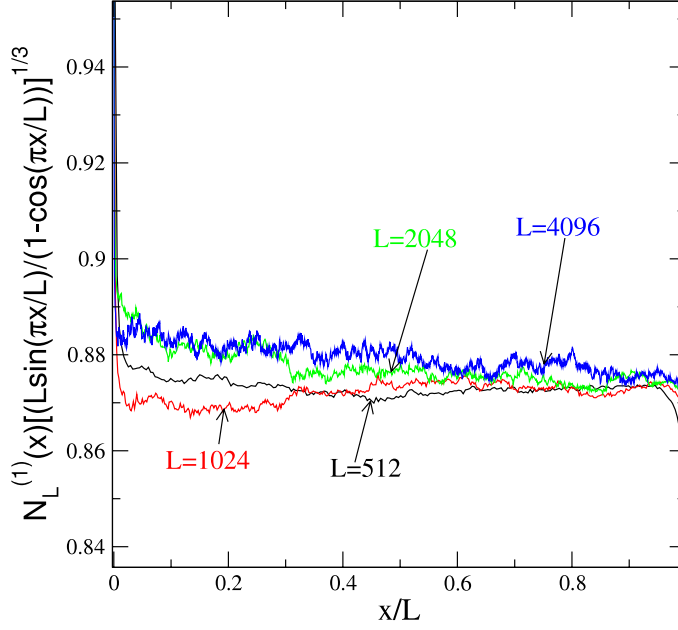


Figure 10. The density of contact points at x for a system of size L , $N_L^{(1)}(x)$ multiplied by $[L \sin(\pi x/L)/(1 - \cos(\pi x/L))]^{1/3}$ for a boundary rate $a = 1$ as a function of x/L for different lattice sizes L (even) = 512, 1024, 2048 and 4096.

would imply that one has to choose p and q in equation (4.1) such that

$$(3p - 2q)^2 = 5, \quad (4.10)$$

which is not possible for any rational values of p and q . On the other hand if one would take $\Delta_{p,q} = 1/3$ and $\bar{\Delta}_{p',q'} = 0$ in equation (4.2) (both values compatible with (4.1)) one would get $X = 1/3$ and $s = 1/3$, a non-zero value of the conformal spin and therefore a vanishing density profile. We have not found an explanation for this puzzle. We are going to see that there is also a second one.

(2) Density of defects.

We consider the RPMW in the defect configurations (see the appendix and figure 5). We have to stress that in the ballot path configurations, defects are non-local observables the same way as contact points are non-local observables in defect configurations. One should add that if one studies the XXZ quantum chain [6], which has the same spectrum as the RPMW, both contact points and defects are non-local observables. In the case of the quantum chain the natural observable could be the local magnetization $\langle \sigma_i^z \rangle$ [21]. One should keep in mind that in the spin basis one loses the probabilistic interpretation of the ground state of the Hamiltonian.

In the defect configurations, the RPMW Hamiltonian acts in the following way. The clusters evolve as in the RPM, adjacent defects (D) annihilate, defects hop over the adjacent clusters peeling them and moving them as a result of the hopping. What we have described up to now can be seen as a pair annihilation process

$$D + D \rightarrow \emptyset \quad (4.11)$$

in unquenched disordered media. This is the situation if the boundary rate $a = 0$ and one has no defects in the stationary state. If the boundary rate is not zero, one injects defects

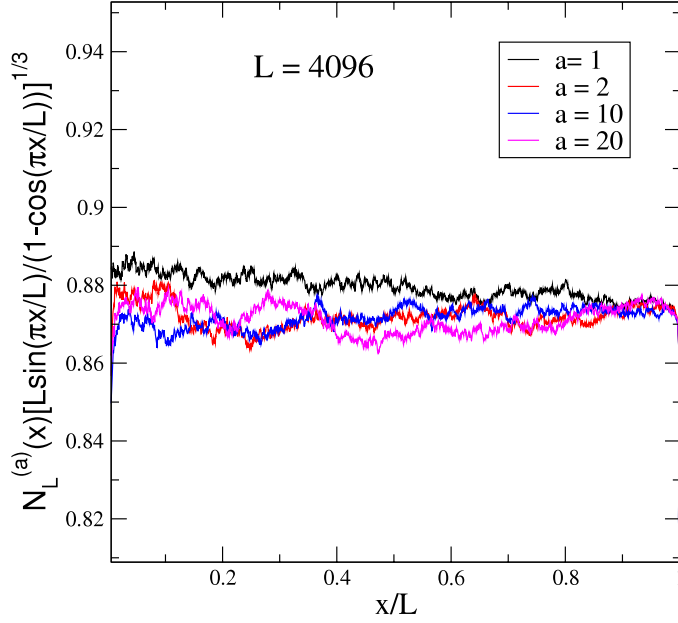


Figure 11. Density of contact points $N_L^{(a)}(x)$ multiplied by $[(L \sin(\pi x/L)/(1 - \cos(\pi x/L))]^{1/3}$ as a function of x/L for L (even) = 4096 and input rates $a = 1, 2, 5, 10$ and 20 .

in the system which compensate for the losses through annihilation and in the stationary states one finds defects and is interested in the density of defects profiles.

For convenience, if a defect is at the point $(x + 1/2)$, x an integer, we will shift it at x .

We expect the density of defects $D_L^{(a)}(x)$ to have an expression like (4.3). As opposed to the density of contact points X is unknown, since the total number of defects, equal to the average height at the origin $\langle h_0 \rangle$ in the ballot path configurations, is not known.

We have observed that one has to consider separately the scaling properties of the density of defects on even and odd sites (denoted by $D_L^{(a)e}(x)$ and $D_L^{(a)o}(x)$ respectively). Monte Carlo simulations on large lattices have shown that the scaling dimension of the local operator corresponding to the defects is:

$$X = 1, \quad (4.12)$$

and therefore one has:

$$D_L^{(a)e/o}(x) = \frac{G^{(a)e/o}(\cos(\pi x/L))}{L \sin(\pi x/L)}. \quad (4.13)$$

In figure 12 one can see the scaling functions for an input rate $a = 1$. Surprisingly, $G^{(1)o}$ has a simple expression but not $G^{(1)e}$. One observes that $G^{(1)e}(1) = G^{(1)o}(1) \simeq 1.75$. This implies that near the source we have the universal behavior:

$$D_L^{(1)}(x) \simeq \frac{1.75}{\pi x} \simeq 0.577 \frac{1}{x} \quad (4.14)$$

for both even and odd sites, and that the total number of defects, equal to $\langle h_0 \rangle_L^{(1)}$ in the

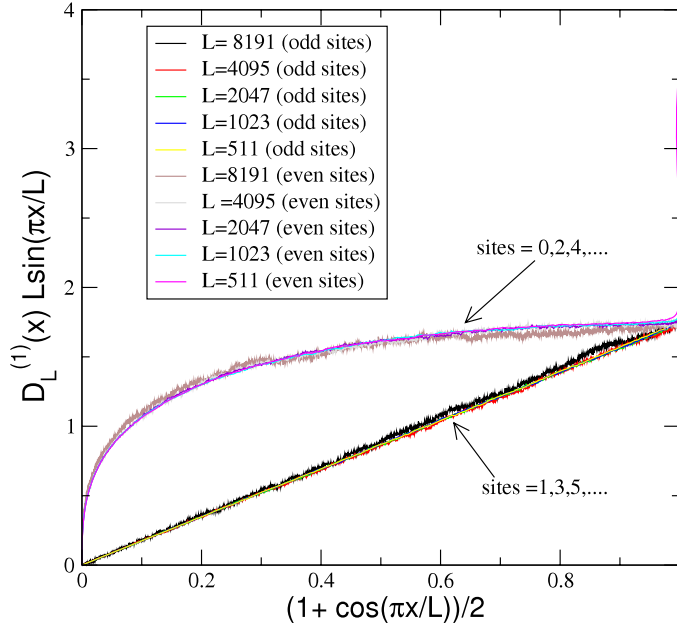


Figure 12. The density of defects $D_L^{(1)}(x)$ multiplied by $L \sin(\pi x/L)$ as a function of $(1 + \cos(\pi x/L))/2$ for different lattice sizes. The profiles for even and odd sites are shown separately.

ballot path picture, increases logarithmically with L . A careful counting gives:

$$\langle h_0 \rangle_L^{(1)} \simeq 0.467 + 0.577 \ln L. \quad (4.15)$$

We have checked that the results presented above are independent of the boundary rate a as expected from conformal invariance. We now try to understand the exponent $X = 1$ (see (4.12)). This would imply (see (4.1) and (4.2)):

$$\Delta_{p,q} = 1/2 \quad \text{and} \quad (3p - 2q)^2 = 13, \quad (4.16)$$

which as in the case of the density of contact points, is not possible. Similar to the previous case, one could take $\Delta_{p,q} = 1$, $\bar{\Delta}_{p',q'} = 0$, both values compatible with (4.1) and get a non-zero conformal spin. Notice that the $1/x$ fall off (4.14) of $D_L^{(1)}(x)$ is the mean-field result for the case in which the hopping is local and symmetric and the input of particles is also local [22]. The same behavior is obtained when fluctuations are taken into account [23]. In our case neither the source acts locally nor is the symmetric hopping local.

(3) *Probability density for the first cluster.*

(a) *The RPM (L even).*

We consider the probability $F_L(x)$ to have the first cluster end at the point x (i.e. the second contact point at x in a Dyck path). In figure 13 we show how this function scales:

$$F_L(x) \simeq f\left(\frac{x}{L}\right) / x^{5/3}. \quad (4.17)$$

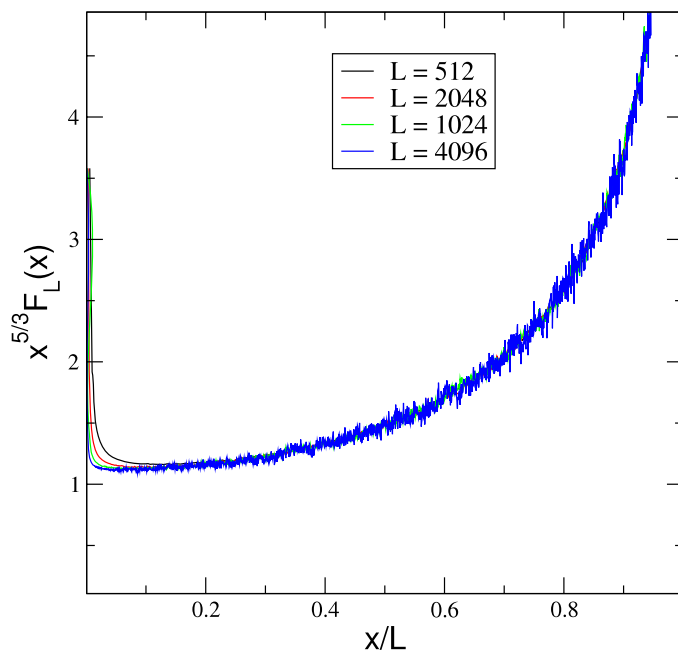


Figure 13. The probability $F_L(x)$ to have the first cluster ending at x in the RPM (L even) multiplied by $x^{5/3}$, as a function of x/L .

This implies that the first cluster increases like $3.3 L^{1/3}$, similar to the average cluster size $1/0.738488L^{1/3} \simeq 1.354118L^{1/3}$ (see (3.8)). No surprises here.

(b) *The RPM and the RPMW for L odd.*

This case is much more interesting. Firstly let us recall that $F_L^{(a)}(x)$ coincides with the probability of having the first cluster end at x in the one-step Dyck path configurations in the RPM model (L odd) (see (3.10) and (3.11)). The latter coincides with the of having the defect at $(x + 1/2)$ in the one-defect configurations. This suggests that $F_L^{(a)}(x, L)$ might have other properties.

Let us consider the following, normalized to 1, probability density function:

$$p(x, L) = \frac{C}{L[\sin(\pi x/L)]^{1/3}}, \quad (4.18)$$

where

$$C = 2\sqrt{\pi}\Gamma(\frac{5}{6})/\Gamma(\frac{1}{3}) \simeq 1.4936. \quad (4.19)$$

In figure 14 we show that in the scaling limit, $F_L^{(a)}(x)$ stays a probability density distribution given by (4.18) for any boundary rate a . This is unexpected and should be understood. Note the reappearance of the exponent $1/3$ in (4.18)

Notice that the first cluster is either small or very big ($p(x, L) = p(L - x, L)$) and that the average size of the first cluster is $L/2$ (this is a linear dependence as opposed to the $L^{1/3}$ dependence in the RPM with L even).

How one can derive a probability density (4.18) from conformal field theory is not clear to us.

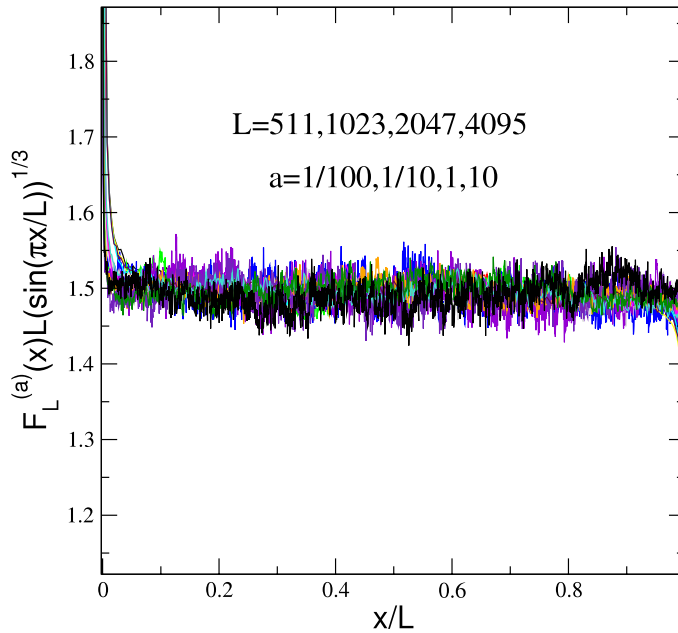


Figure 14. The probability distribution function to have the first cluster ending at x , for a system of size L , $F_L^{(a)}(x)$ multiplied by $L(\sin(\pi x/L))^{1/3}$ as a function of x/L for different values of L and boundary rates a .

One of the most interesting aspects of our study is the deep connection between the RPM for L odd (one-step Dyck paths) and the RPMW model in the defect configurations (corresponding to ballot paths). The rightmost defect behaves like the single defect which defines the position of the leftmost cluster in the RPM (one-step Dyck paths picture). Like the single defect, the rightmost defect makes Lévy flights and behaves like a ‘relativistic’ random walker [8]. The physics to the right of the leftmost cluster is identical in both cases, therefore the density of contact points in the two models is the same. The difference between the two models is all in the first cluster. In the RPMW model one has defects in the first cluster, while in the RPM there are no defects. The content of the first cluster in the RPM can be easier understood in the one-defect picture in which the time-evolution operator acts in the left–right symmetric way.

Before closing this section, let us discuss shortly the implication of the conjectures (3.16) for $A_L^{(1)}$, the average number of local minima of the interface divided by L in the RPMW. In the large L limit one obtains

$$A_L^{(1)} \xrightarrow{L \rightarrow \infty} 3/8. \quad (4.20)$$

This number is identical with the one observed in the RPM (L even) [1]. This implies (see [1]) that the average number of tiles desorbed in avalanches is again 1.5. This coincidence suggests that most of the desorption processes take place within the clusters. The different cluster structures in the RPM and the RPMW, do not affect most of the avalanches. This does not imply that the rare large avalanches [2] are the same in the two models.

5. The raise and peel model with and without a wall in continuous time. Temperley–Lieb algebras

In this section we show how the RPM and RPMW described in section 2 were obtained. We also give the necessary background to derive the exact results given in section 3 and derived in sections 7 and 8.

The continuous time evolution of a system composed of the states $\alpha = 1, 2, \dots, n$ with probabilities $P_\alpha(t)$ is given by a master equation that can be interpreted as an imaginary time Schrödinger equation:

$$\frac{d}{dt}P_\alpha(t) = - \sum_{\beta} H_{\alpha,\beta}P_\beta(t), \quad (5.1)$$

where the Hamiltonian H is an $n \times n$ intensity matrix: $H_{\alpha,\beta}$ non-positive ($\alpha \neq \beta$) and $\sum_{\alpha} H_{\alpha,\beta} = 0$. $-H_{\alpha,\beta}$ is the rate for the transition $|\beta\rangle \rightarrow |\alpha\rangle$. The ground state eigenvector of the system $|0\rangle$, $H|0\rangle = 0$, gives the probabilities in the stationary state:

$$|0\rangle = \sum_{\alpha} P_{\alpha}|\alpha\rangle, \quad P_{\alpha} = \lim_{t \rightarrow \infty} P_{\alpha}(t). \quad (5.2)$$

The normalization factor of the unnormalized probabilities P_{α} is $\langle 0|0\rangle$ where

$$\langle 0| = \sum_{\alpha} \langle \alpha|, \quad \langle 0|H = 0. \quad (5.3)$$

Since H is an intensity matrix, the real parts of the n eigenvalues E_{α} are non-negative and, if complex, the eigenvalues come in conjugate pairs. The eigenvalue zero is not degenerate.

For our present purposes we need the following observation [3]: if g_i ($i = 1, \dots, p$) are generators of a semigroup algebra, then:

$$H = \sum_{i=1}^p a_i(1 - g_i) \quad (5.4)$$

acting from the left in the vector space defined by the regular representation or by a left ideal of the algebra, is an intensity matrix (a_i are non-negative real numbers).

In the following we are going to use the Temperley–Lieb (TL) and the one-boundary Temperley–Lieb semigroup algebras.

The Temperley–Lieb algebra \mathcal{T}_L [9] is given by a set of $(L - 1)$ generators e_i , $i = 1, \dots, L - 1$, subject to relations

$$e_i^2 = \tau e_i, \quad e_i e_{i\pm 1} e_i = e_i, \quad e_i e_j = e_j e_i \quad \text{if } |i - j| > 1. \quad (5.5)$$

Here τ is the parameter of the algebra which for our applications we put equal to one: $\tau = 1$. We notice that with this choice all structure constants of the algebra become units and the TL algebra becomes a semigroup algebra (see [3]).

The one-boundary extension of the Temperley–Lieb algebra $\mathcal{T}_L^{(1B)}$ (also known under the name of blob algebra [5]) is obtained by adding a boundary generator e_0 satisfying relations

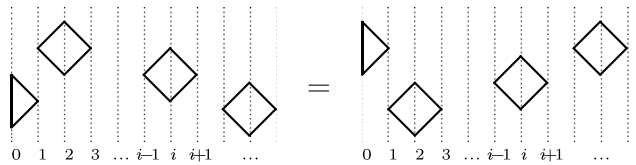
$$e_0^2 = \omega e_0, \quad e_1 e_0 e_1 = e_1, \quad e_0 e_i = e_i e_0 \quad \forall i > 1. \quad (5.6)$$

We fix again the parameter $\omega = 1$ and get a semigroup algebra.

For our purposes it is convenient to represent the generators e_i and the boundary generator e_0 as, respectively, tiles and a half-tile:

$$e_i = \begin{array}{c} \diagup \\ \diamond \\ \diagdown \\ \vdots \\ i \end{array}, \quad e_0 = \begin{array}{c} \diagup \\ \triangleright \\ \vdots \\ 0 \end{array}. \quad (5.7)$$

The tiles and the half-tile are placed on labeled vertical lines and they can move freely along the lines unless they meet other (half-)tiles:



Multiplication in the algebra corresponds to a simultaneous placement of several (half-) tiles on the same picture and an order of the product corresponds to moving the tiles downwards. Thus, the picture above corresponds to the commutation relations in (5.5) and (5.6). The remaining relations in (5.5) and (5.6) are equivalent to the following pictures

$$\begin{array}{c} \begin{array}{c} \diagup \\ \diagdown \\ \vdots \\ i-1 \end{array} \begin{array}{c} \diagdown \\ \diagup \\ \vdots \\ i \end{array} \\ \vdots \\ \dots \end{array} = \begin{array}{c} \begin{array}{c} \diagdown \\ \diagup \\ \vdots \\ i-1 \end{array} \begin{array}{c} \diagup \\ \diagdown \\ \vdots \\ i \end{array} \\ \vdots \\ \dots \end{array} = \begin{array}{c} \begin{array}{c} \diagup \\ \diagdown \\ \vdots \\ i-1 \end{array} \begin{array}{c} \diagdown \\ \diagup \\ \vdots \\ i \end{array} \\ \vdots \\ \dots \end{array} = \begin{array}{c} \diamond \\ \vdots \\ i \end{array}, \quad (5.8)$$

$$\begin{array}{c} \begin{array}{c} \diagup \\ \vdots \\ 0 \end{array} \begin{array}{c} \diagup \\ \vdots \\ 1 \end{array} \\ \vdots \\ \dots \end{array} = \begin{array}{c} \begin{array}{c} \diagup \\ \vdots \\ 0 \end{array} \\ \vdots \\ \dots \end{array}, \quad \begin{array}{c} \begin{array}{c} \diagdown \\ \diagup \\ \vdots \\ 0 \end{array} \begin{array}{c} \diagup \\ \diagdown \\ \vdots \\ 1 \end{array} \\ \vdots \\ \dots \end{array} = \begin{array}{c} \diamond \\ \vdots \\ 1 \end{array}. \quad (5.9)$$

We consider now the following projectors in the TL and the one-boundary TL algebras:

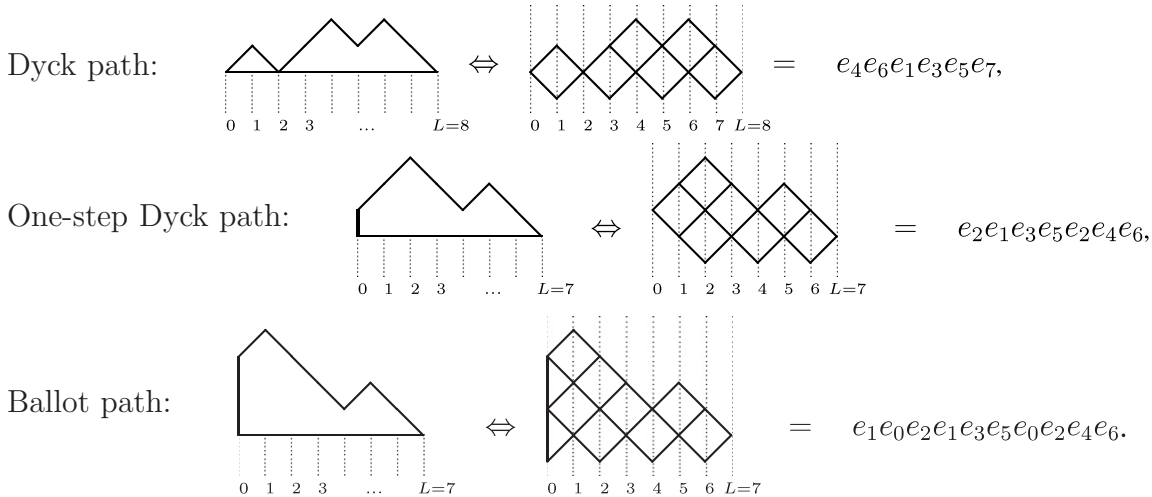
$$\left. \begin{array}{l} \text{Temperley-Lieb algebra and} \\ \text{one-boundary TL algebra,} \end{array} \right\} L \text{ even: } \begin{array}{c} \begin{array}{c} \diagup \\ \diagdown \\ \vdots \\ 0 \end{array} \begin{array}{c} \diagdown \\ \diagup \\ \vdots \\ 1 \end{array} \begin{array}{c} \diagup \\ \diagdown \\ \vdots \\ 2 \end{array} \dots \begin{array}{c} \diagup \\ \diagdown \\ \vdots \\ L-1 \end{array} \begin{array}{c} \diagdown \\ \diagup \\ \vdots \\ L \end{array} \\ \vdots \\ \dots \end{array} = e_1 e_3 \dots e_{L-1},$$

$$\text{Temperley-Lieb algebra, } L \text{ odd: } \begin{array}{c} \begin{array}{c} \diagup \\ \diagdown \\ \vdots \\ 0 \end{array} \begin{array}{c} \diagdown \\ \diagup \\ \vdots \\ 1 \end{array} \begin{array}{c} \diagup \\ \diagdown \\ \vdots \\ 2 \end{array} \begin{array}{c} \diagdown \\ \diagup \\ \vdots \\ 3 \end{array} \dots \begin{array}{c} \diagup \\ \diagdown \\ \vdots \\ L-1 \end{array} \begin{array}{c} \diagdown \\ \diagup \\ \vdots \\ L \end{array} \\ \vdots \\ \dots \end{array} = e_2 e_4 \dots e_{L-1},$$

$$\text{One-boundary TL algebra, } L \text{ odd: } \begin{array}{c} \begin{array}{c} \diagdown \\ \diagup \\ \vdots \\ 0 \end{array} \begin{array}{c} \diagup \\ \diagdown \\ \vdots \\ 1 \end{array} \begin{array}{c} \diagdown \\ \diagup \\ \vdots \\ 2 \end{array} \begin{array}{c} \diagup \\ \diagdown \\ \vdots \\ 3 \end{array} \dots \begin{array}{c} \diagup \\ \diagdown \\ \vdots \\ L-1 \end{array} \begin{array}{c} \diagdown \\ \diagup \\ \vdots \\ L \end{array} \\ \vdots \\ \dots \end{array} = e_0 e_2 e_4 \dots e_{L-1}.$$

We multiply the projectors by all elements of the respective algebras from the left (that is, dropping the (half-)tiles downwards) and generate in this way left ideals (left-invariant subspaces in the algebras). The projectors are non-invertible and therefore the ideals are smaller than the algebras themselves. The dimensions of the resulting ideals are: C_L (see equation (2.2)) for the TL algebra for L even, C_{L+1} for the TL algebra for L odd, and $\binom{L}{\lfloor L/2 \rfloor}$ for the one-boundary TL algebra. These dimensions coincide with the numbers of the Dyck paths, one-step Dyck paths and the ballot paths, respectively. One can easily

see a correspondence between the paths and the pictures of words in the ideals. The correspondence is illustrated below.



Obviously, the projectors correspond to the substrates in the figures 1, 2 and 4 (see section 2).

The Hamiltonian governing the time fluctuations of the RPM and the RPMW are given by the following expressions (see (5.4))

$$H_L = \sum_{i=1}^{L-1} (1 - e_i), \quad H_L^{(a)} = a(1 - e_0) + \sum_{i=1}^{L-1} (1 - e_i), \quad (5.10)$$

where a is the boundary rate.

We now notice that the multiplication of the words from the ideals by the generators e_i and e_0 drawn in pictures according to the rules (5.8) and (5.9) coincides with the elementary processes (adsorption, reflection and desorption) of the RPM and the RPMW models.

The ground state eigenvectors of the two intensity matrices (5.10) have remarkable combinatorial properties [11]–[15], [24, 25]. New combinatorial aspects of these ground state eigenvectors are going to be shown in sections 7 and 8 and will be used to derive the results enumerated in section 3.

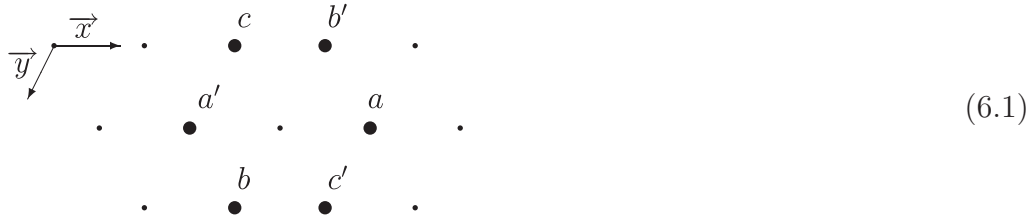
One can use the representation of the generators e_0, e_i in terms of the Pauli matrices to derive exact results. In this representation H_L and $H_L^{(a)}$ are given by XXZ spin-half quantum chain Hamiltonians with non-Hermitian boundary terms [16]. From the finite-size scaling limit of the Hamiltonian eigenspectra we can derive the conformal properties of the systems [10, 6].

6. Hexagon recurrence relations

In this section we want to show that the expressions (3.1) and (3.2) for $S(L, n)$ and $P(L, n, m)$ are solutions of two recurrence relations. They can be seen as generalizations of the recurrence relations obtained from the Pascal triangle. This section is pure mathematics. The connection with the RPM and RPMW is going to be made in sections 7 and 8.

6.1. Pascal's hexagon

Let us place numbers on the sites of a trigonal lattice in such a way that any six numbers, occupying the vertices of an elementary hexagon as shown on the figure below,



satisfy the relation

$$c' c = a' a + b' b. \tag{6.2}$$

Introducing a coordinate frame $\{\vec{x}, \vec{y}\}$ on the lattice (see figure above) and denoting $S(L, n)$ the number associated to a vertex $(L\vec{x} + n\vec{y})$ we can write the relation (6.2) in the form

$$S(L + 1, n + 1) S(L - 1, n - 1) = S(L - 1, n) S(L + 1, n) + S(L, n - 1) S(L, n + 1). \tag{6.3}$$

This equation was obtained in [26] as a discretized version of the Boussinesq equation. It is a particular two-dimensional reduction of the three-dimensional discrete Hirota equation (see [27, 28] and references therein) which is also known as the octahedron recurrence in combinatorics (see [29] and references therein).

We treat (6.3) as a recurrence relation which gives the number $S(L + 1, n + 1)$ (corresponding to c' in the figure) in terms of the numbers placed in the two upper rows (respectively, a, a', c and b') and at the left neighbor site from the same row (resp., b). We solve the recurrence relation by moving rightwards in a row and downwards row by row. Taking the following set of initial data

$$S(L, -1) = S(L, 0) = 1, \quad S(2n - 1, n) = 0 \quad \forall n > 0 \tag{6.4}$$

we can calculate numbers $S(L, n)$ in a sector $n \geq -1, L \geq 2n - 1$. As far as we know these boundary conditions were not considered before.

The values of $S(L, n)$ for small L and n are given in figure 15. This figure and the recursive procedure described above reminds of the famous Pascal's triangle rule—an arrangement of the binomial coefficients in a triangle. A closer inspection of the solution adds more arguments in favor of such an analogy. First, we notice that all numbers on figure 15 are integers, which is not trivial since solving the recurrence relation (6.3) one obtains ratios⁵. Moreover, all the numbers in figure 15 can be factorized into relatively small primes (compared to the numbers themselves). For example $S(9, 4), S(10, 5)$ and $S(12, 5)$ are given respectively by:

$$7429 = 17 \cdot 19 \cdot 23, \quad 45\,885 = 3 \cdot 5 \cdot 7 \cdot 19 \cdot 23, \quad 9304\,650 = 2 \cdot 3^2 \cdot 5^2 \cdot 23 \cdot 29 \cdot 31.$$

This factorization property suggests an idea to look for an expression of $S(L, n)$ in terms of factorials, just as it is the case for the binomial coefficients. The solution of the recurrence relation (6.3), with initial condition (6.4), is given by (3.1) [14].

⁵ For a general discussion of such phenomena see [30].

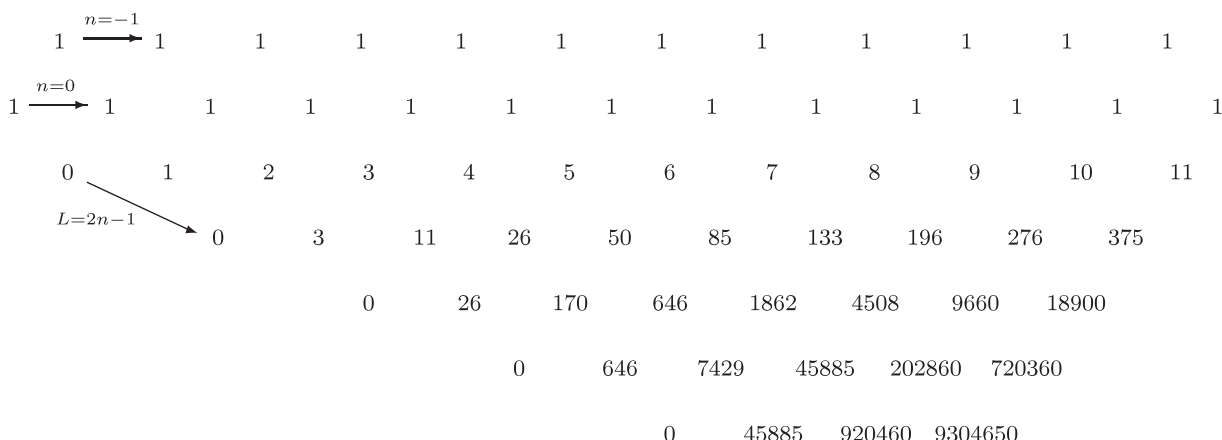


Figure 15. Pascal's hexagon rule.

One can look for a more general solution of the Pascal's hexagon recurrence (6.3) using the initial conditions depending now on a parameter a :

$$S^{(a)}(L, -1) = 1, \quad S^{(a)}(L, 0) = a^{\delta_{L,0}}, \quad S^{(a)}(2n - 1, n) = 0 \quad \forall n > 0. \quad (6.5)$$

Remarkably again, all the quantities $S^{(a)}(L, n)$ in the sector $n \geq -1, L \geq 2n - 1$, turn out to be polynomials in variable a with integer coefficients. These polynomials are particular examples of the polynomial solutions considered in the appendix of [14] ($S^{(a)}(L, n) = F_{L,n}(x = 1, y = a)$ in the notation of [14]). The polynomials $S^{(a)}(L, n)$ can be also observed in the stationary states of the RPMW with an arbitrary boundary rate a (see section 8). Obviously, one has $S^{(1)}(L, n) = S(L, n)$.

6.2. Split hexagon

We now introduce a vertical direction \vec{z} in the picture (6.1) and put numbers $P(L, n, m)$ into correspondence with the vertices $(L\vec{x} + n\vec{y} + m\vec{z})$ of the 3d lattice (see figure 16). We impose the following relations on $P(L, n, m)$'s:

$$\sum_{m=0}^n P(L, n, m) = S(L, n), \quad (6.6)$$

$$P(L, n, -k) = P(L, n, n + k) = 0 \quad \forall k > 0, \quad n \geq 0, \quad (6.7)$$

and the equations

$$P(L + 1, n + 1, m) S(L - 1, n - 1) = P(L - 1, n, m) S(L + 1, n) + P(L, n - 1, m - 2) S(L, n + 1). \quad (6.8)$$

Summing over m the relations (6.8) one obtains the hexagon relations (6.3), therefore we call (6.8) the *split-hexagon* relations.

Taking into account (6.6), the equation (6.8) defines recurrence relations for the $P(L, n, m)$'s. Indeed, using (6.7) and the initial conditions (cf with the initial data (6.4))

$$P(L, 0, m) = \delta_{m,0}, \quad P(L, -1, m) = \delta_{m,-1}, \quad \text{and} \quad P(2n, n, m) = 0 \quad \forall m > 1, \quad (6.9)$$

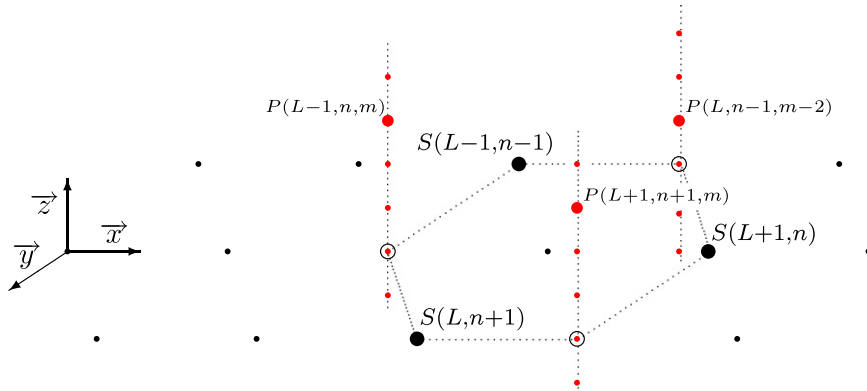


Figure 16. Split hexagon: the numbers $S(L + 1, n + 1)$, $S(L - 1, n)$ and $S(L, n - 1)$ split, respectively, into the parts $P(L + 1, n + 1, m)$, $P(L - 1, n, m)$ and $P(L, n - 1, m)$, $m = 0, 1, \dots$

one can calculate the numbers $P(L, n, m)$ starting from the row $n = 1$ downwards and moving rightwards from the point $L = 2n$ in a row. For each given pair L and n one calculates $P(L, n, m)$ for all $m = 0, 1, \dots, n$.

We notice that the split-hexagon recursion is a kind of ‘bootstrap’ procedure as after each step (for example, the calculation of $P(L, n + 1, m)$ for all $m = 0, 1, \dots, n + 1$) one has to find a coefficient for the equations which are solved at the next step of the recursion (that is, the coefficient $S(L, n + 1) = \sum_{m=0}^{n+1} P(L, n + 1, m)$ in the equations for $P(L + 1, n + 1, m)$). We also remark that there is no need to set the boundary values

$$P(2n, n, 0) = S(2n, n - 1) \quad \text{and} \quad P(2n, n, 1) = 0$$

as they are completely defined by the data from the previous $(n - 1)$ th row only (the last term in the split-hexagon relation (6.8) vanishes for $m = 0$ or 1).

The relations (6.8) are new and can be generalized changing the condition (6.6). The continuous version of (6.8) is not yet known.

The solution of the split-hexagon recursion is given by integer numbers with simple factorization properties, e.g.,

$$\begin{aligned} P(12, 4, 2) &= 2041\,020 = 2^2 \cdot 3^2 \cdot 5 \cdot 17 \cdot 23 \cdot 29, \\ P(12, 4, 3) &= 2281\,140 = 2^2 \cdot 3^2 \cdot 5 \cdot 19 \cdot 23 \cdot 29. \end{aligned}$$

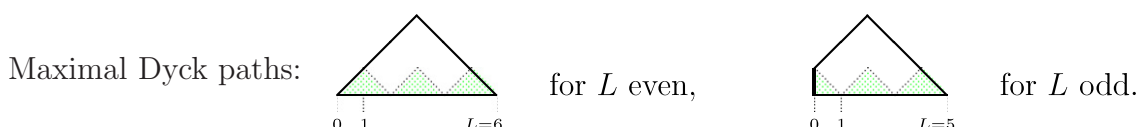
This suggests the $P(L, n, m)$ ’s can be written as a product of factorials. One can show that the expression given by (3.2) for $P(L, n, m)$ is the solution of the split-hexagon recurrence relations (6.6) and (6.8) with the boundary conditions (6.7) and (6.9).

7. Combinatorics in the stationary states of the RPM

We have shown in the last section that the quantities $P(L, n, m)$ are solutions of the split-hexagon recurrence relations (6.8) and we gave their expression (3.2). We now make the connection with the stationary states of the RPM⁶.

⁶ Actually it was by observing the combinatorial properties of the RPM’s stationary states that we were led to the hexagon and the split-hexagon relations.

The stationary state of the RPM for a system of size L is described by the eigenvector $|0\rangle_L$ of the operator H_L (5.10) corresponding to eigenvalue zero. It is a linear combination of the words in the Dyck path representation (see section 5) defined up to a common constant factor. A suitable normalization for $|0\rangle_L$ is to set the coefficient of the maximal Dyck path (see figures below) to be equal to 1.



This is the smallest coefficient in the vector $|0\rangle_L$ and the corresponding profile is the least probable in the stationary state. With this choice, all the weights of the different Dyck paths in the ground state eigenvectors are integer numbers which can be related to an enumeration of loops in a fully packed loops ice model [24]. The most probable stationary configuration is the substrate shown as a dashed region on the figures above⁷.

Consider a Dyck path with L sites. Let h be a number from the list

$$0, 1, \dots, \left\lfloor \frac{L-1}{2} \right\rfloor,$$

such that the Dyck path has no local minima (return points) below the height h . (See figure 17.) Let us denote by m ($m \geq 0$) the number of returns at the height h for a given path. We consider all the configurations which have m return points at the height h and the remaining ones higher.

Conjecture. *The sum of all the coefficients in $|0\rangle_L$ corresponding to these configurations is given by $P(L, n, m)$. Here*

$$n = \left\lfloor \frac{L-1}{2} \right\rfloor - h, \quad n = 0, 1, \dots, \left\lfloor \frac{L-1}{2} \right\rfloor, \quad \text{and} \quad m = 0, 1, \dots, n. \quad (7.1)$$

n counts the height from the top of the triangle instead of its basis.

This conjecture was checked for lattices of size $L \leq 13$. There are more consistency checks for this conjecture:

- One clearly has $P(L, n+1, 0) = \sum_{m=0}^n P(L, n, m) = S(L, n)$ (see (6.6)), which is the sum of all the coefficients in $|0\rangle_L$ corresponding to the configurations with local minima at values higher or equal to $h = (\lfloor (L-1)/2 \rfloor - n)$ and is given by (3.1). This expression was conjectured earlier and checked independently on small lattices in [13, 14].
- More importantly, it was proven analytically in [31, 32] that $S(L)$ (see (3.3) and (3.4)) coincides with the normalization factor (sum of all the weights) of $|0\rangle_L$:

$${}_L \langle 0 | 0 \rangle_L = S(L) = S(L, \lfloor (L-1)/2 \rfloor). \quad (7.2)$$

The expression for the probability of having k clusters for a system of size L given in section 3 (see (3.5)) is an obvious corollary of the conjecture.

⁷ Intuitively, the more reflection points (local maxima) one has in a profile, the larger is its contribution to the stationary state.

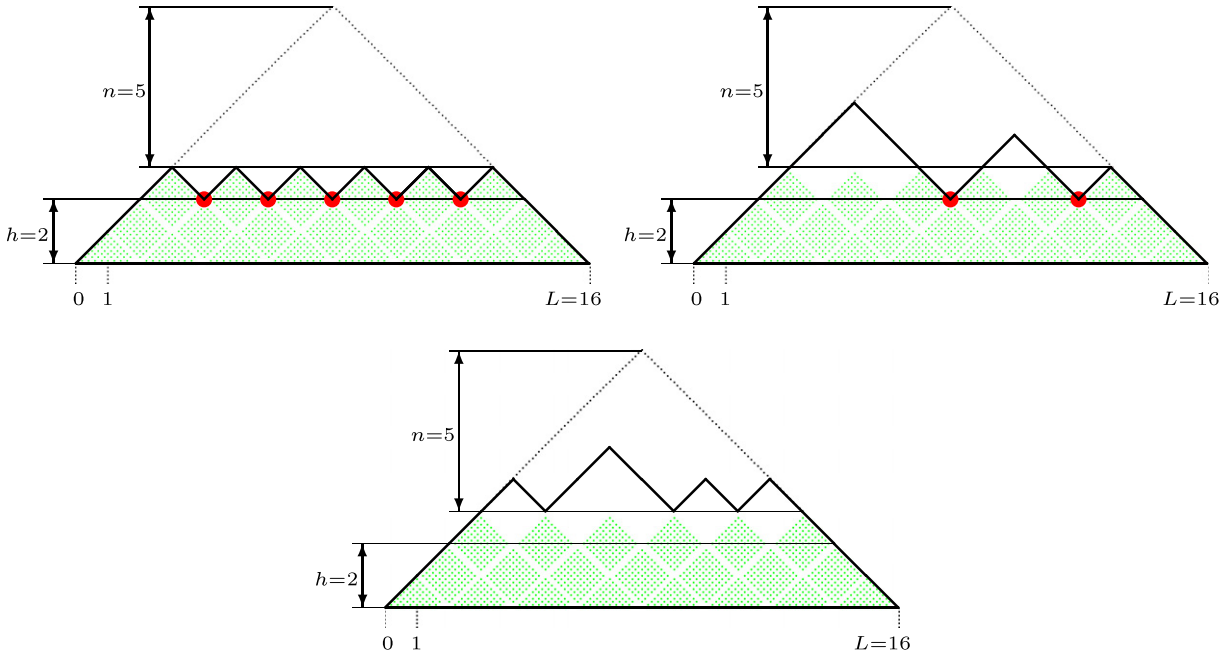
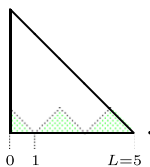


Figure 17. Examples of Dyck paths of the size $L = 16$ satisfying the selection criteria for $h = 2 \Leftrightarrow n = 5$. The number m of return points at the height $h = 2$ (red points on the pictures) is equal, respectively, to 5, 2, and 0.

8. Clusters in the stationary states of the RPMW and RPM

In this section we prove the expressions (3.6) and (3.7) for the probabilities to have k clusters for a system of size L as well the relations (3.10)–(3.13) for the probability densities observed in the RPMW. To this end we make use of the algebraic background (the TL algebras described in section 6), and of the conjecture presented in section 7.

The stationary state of the RPMW for a system of size L is described by the ground state eigenvector of the operator $H_L^{(a)}$ (5.10) which is a linear combination of the words in the ballot path representation (see section 5) with coefficients (weights) depending on the boundary rate a . We use a notation $|0\rangle_L^{(a)}$ for this eigenvector and, if necessary, we explicitly show the value of a in the notation, say $|0\rangle_L^{(1)}$ for $a = 1$. A suitable normalization for $|0\rangle_L^{(a)}$ is to set the coefficient of the maximal ballot path (see figure below) to be equal to $a^{\lfloor L/2 \rfloor}$. In case $a = 1$ it is the smallest coefficient in $|0\rangle_L^{(1)}$.

Maximal ballot path:  (8.1)

With this choice, all the weights of the different ballot paths in the ground state eigenvectors become polynomials in a with integer coefficients which can be related to a ‘weighted’ enumeration of loops in a fully packed loops ice model [15]. As it was proven in [32], in the case $a = 1$, the normalization factor (sum of all weights) of $|0\rangle_L^{(1)}$ is equal

to the number of vertically and horizontally symmetric alternating sign matrices of a size $(2L + 3)$ (see (3.3) and (3.4))

$${}_L^{(1)}\langle 0|0\rangle_L^{(1)} = A_{2L+3}^{\text{VH}} = S(L) S(L + 1). \tag{8.2}$$

For an arbitrary boundary rate a , the normalization factor reads (see [32], equation (4.8))

$${}_L^{(a)}\langle 0|0\rangle_L^{(a)} = S(L) S^{(a)}(L + 1). \tag{8.3}$$

Here $S^{(a)}(L) = S^{(a)}(L, \lfloor (L - 1)/2 \rfloor)$, and $S^{(a)}(L, n)$ is a polynomial solution of the Pascal's hexagon recurrence (6.3) with the initial conditions (6.5).

Now we are going to use homomorphisms from the one-boundary TL algebra $\mathcal{T}_L^{(1B)}$ to the TL algebras \mathcal{T}_L and \mathcal{T}_{L+1} to establish relations between the ground state vectors of the RPM models with and without a wall. One has to consider the cases L even and odd separately.

8.1. Case of L odd

We consider the homomorphism between the one-boundary TL algebra and the TL algebra (see (5.5) and (5.6)) of the same size L , defined by

$$\mathcal{T}_L^{(1B)} \rightarrow \mathcal{T}_L: \quad e_0 \mapsto 1, \quad e_i \mapsto e_i \quad \forall i = 1, \dots, L - 1. \tag{8.4}$$

This homomorphism maps the intensity matrix of the RPMW (a is arbitrary) onto the intensity matrix of the RPM for the same number of sites L (see (5.10))

$$H_L^{(a)} \mapsto H_L, \tag{8.5}$$

and so should map their unique ground state eigenvectors:

$$|0\rangle_L^{(a)} \mapsto S^{(a)}(L + 1) |0\rangle_L, \tag{8.6}$$

where we have computed the scaling constant $S^{(a)}(L + 1)$ by comparing the expressions for normalization factors (7.2) and (8.3).

Let us consider in more details an action of the map (8.6) on a ballot path. Graphically one can realize this mapping using the following procedure (see figure 18): one first erases all the half-tiles from the picture of the ballot path and then, one reduces the resulting expression using the rules (5.8) (actually one needs only the last equality from (5.8)). There can be several ballot paths mapping onto the same one-step Dyck path under this procedure. One can reconstruct the corresponding ballot paths by dressing the one-step Dyck path with the layers of tiles starting at any of its return point (local minima) at height $h = 1$ in the first cluster and ending by a half-tile at the wall (see figure 18). Assuming there are r such return points in the one-step Dyck path, one can construct 2^r different 'dressed' ballot paths.

We observe that the profiles of all the ballot paths mapping under (8.4) onto the same Dyck path coincide except for their leftmost clusters. They are identical to the profile of the corresponding Dyck path, again, with an exception of its leftmost cluster. We now notice that, according to (8.6), in the RPMW (L odd) the stationary weights of the ballot paths mapping to the same Dyck path sum up (modulo the constant factor) $S^{(a)}(L + 1)$ to the stationary weight of the corresponding Dyck path in the RPM (same size L). These two observations justify the following statement.

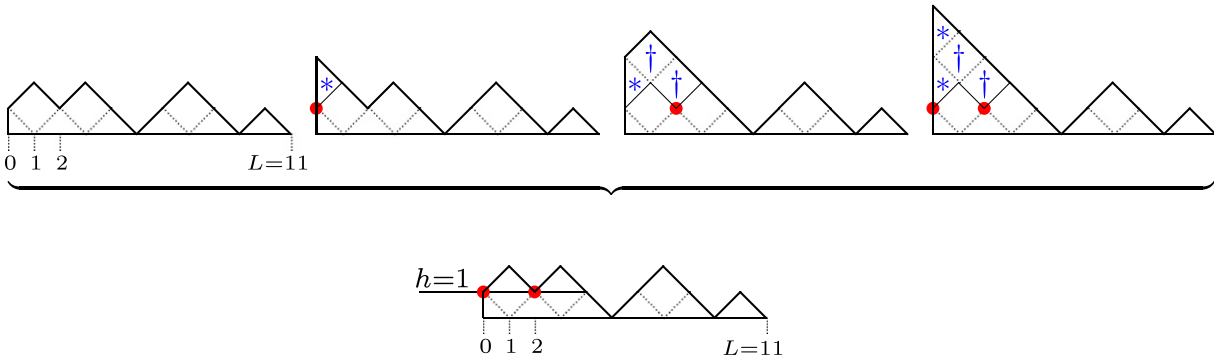


Figure 18. Four different ballot paths (shown on top) map to the same one-step Dyck path (shown below) under the homomorphism (8.4). Marked by asterisk ‘*’ are the half-tiles which one erases during the mapping. Marked by dagger ‘†’ are the tiles which one then removes using the rule (5.8). There are $r = 2$ reflection points at height $h = 1$ in the first cluster of the one-step Dyck path (see marked points). Therefore, one finds $2^r = 4$ different ballot paths in the preimage. The starting points for the layers of tiles are marked on the pictures of ballot paths.

Proposition 1. Consider the RPM and the RPMW for the same number of sites L (L odd) and any boundary rate a . For both models the stationary probabilities to have the first cluster at distance x and any given configuration to the right of it are the same.

In particular, for L odd, the relations (3.10) and (3.12) are valid and the conjecture announced earlier implies the equality (3.6).

8.2. Case of L even

In this case we restrict our consideration to the case $a = 1$ only. We consider another homomorphism mapping the one-boundary TL algebra of size L onto the TL algebra of size $(L + 1)$:

$$\mathcal{T}_L^{(1B)} \rightarrow \mathcal{T}_{L+1}: \quad e_0 \mapsto e_1, \quad e_i \mapsto e_{i+1} \quad \forall i = 1, \dots, L - 1. \quad (8.7)$$

This homomorphism maps the intensity matrix of the RPMW, $a = 1$, to the intensity matrix of the RPM

$$H_L^{(1)} \mapsto H_{L+1}, \quad (8.8)$$

and so should map their unique ground state eigenvectors:

$$|0\rangle_L^{(1)} \mapsto S(L) |0\rangle_{L+1}, \quad (8.9)$$

where we have computed the scaling constant $S(L)$ by comparing the expressions for their normalization factors (7.2) and (8.2).

With respect to the action of homomorphism (8.7) the set of even size L ballot paths separates naturally into two parts.

- (a) The ballot paths which have zero height at the origin, $h_0 = 0$, map onto the one-step Dyck paths with $h_1 = 0$ (see figure 19). The mapping (8.7) on these subsets of paths is a one to one correspondence.

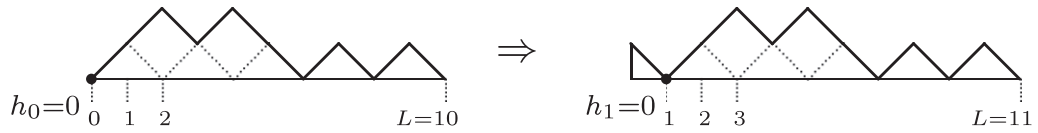


Figure 19. A ballot path which has height 0 at the wall maps under the homomorphism (8.7) to the one-step Dyck path with $h_1 = 0$. There are no other ballot paths mapping to this Dyck path.

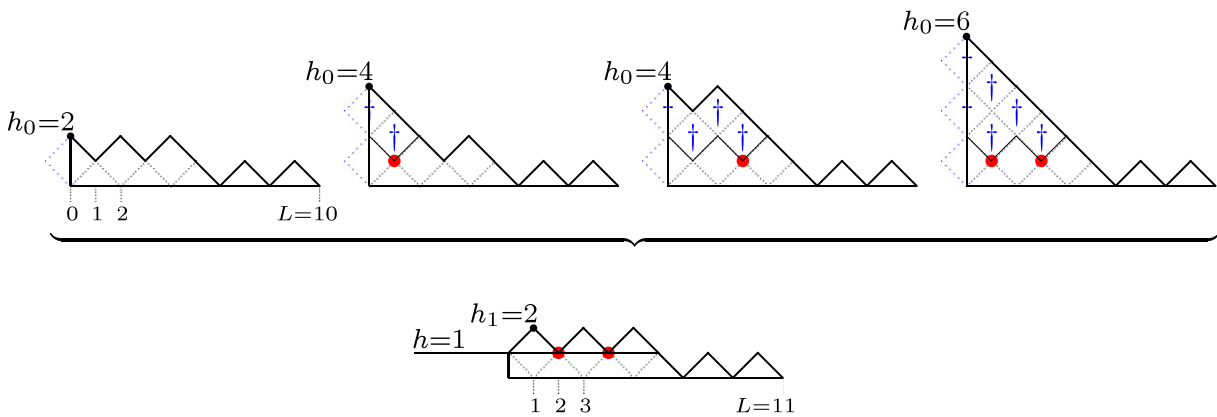


Figure 20. Four different ballot paths (shown on top) map to the same one-step Dyck path (shown below) under the homomorphism (8.7). The half-tiles on the pictures of ballot paths are completed to full tiles. Marked by dagger ‘†’ are the tiles which one removes during the mapping using the rule (5.8). There are $r = 2$ reflection points at height $h = 1$ (h_0 excluded) in the first cluster of the one-step Dyck path (see marked points). Therefore, one finds $2^r = 4$ different ballot paths in the preimage. The starting points for the layers of tiles are marked on the pictures of ballot paths.

- (b) The ballot paths which have heights $h_0 = 2, 4, \dots, L/2$ at the origin map onto the one-step Dyck paths with $h_1 = 2$ (see figure 20). Graphically one can realize the map (8.7) for such paths in the following way: firstly, one completes each half-tile on the picture of the ballot path to a full tile and then, one reduces the resulting expression using the rules (5.8) (one needs only the last equality from (5.8)). This map is not a one to one correspondence. The number of ballot paths in the preimage of a given restricted, $h_1 = 2$, one-step Dyck path is equal to 2^r , where r is the number of return points at height $h = 1$ in the first cluster of the one-step Dyck path, the point $h_0 = 1$ is excluded (see figure 20). The reconstruction of the preimage in this case is obtained again, by dressing the one-step Dyck path with layers touching the wall (see caption of figure 20).

We observe that in both cases (a) and (b), the profiles of the ballot paths, except their leftmost clusters, are identical to the profiles of the corresponding one-step Dyck paths. We also notice that the leftmost clusters become one step larger under the map (8.7).

Therefore, taking into account the relation (8.9) we conclude:

Proposition 2. *For the RPMW of even size L and the boundary rate $a = 1$, the stationary probability of having the first cluster at distance x and any given configuration to the right of it is equal to the stationary probability for the RPM of odd size $(L + 1)$, to have the first cluster at distance $(x + 1)$ and the same configuration to the right of it.*

In particular, the relations (3.11) and (3.13) are satisfied.

Finally, we demonstrate that the proposition 2, together with the conjecture presented in page 26 implies the equality (3.7). Taking into account that the ballot paths with k clusters project under (8.7) to the one-step Dyck paths with $(k + 1)$ clusters in case (a) (see figure 19) and with k clusters in case (b) (see figure 20) one can write

$$L \text{ even: } P_L^{(1)}(k) = P_{L+1}(k, h_1 = 2) + P_{L+1}(k + 1, h_1 = 0) \\ = P_{L+1}(k) - P_{L+1}(k, h_1 = 0) + P_{L+1}(k + 1, h_1 = 0), \tag{8.10}$$

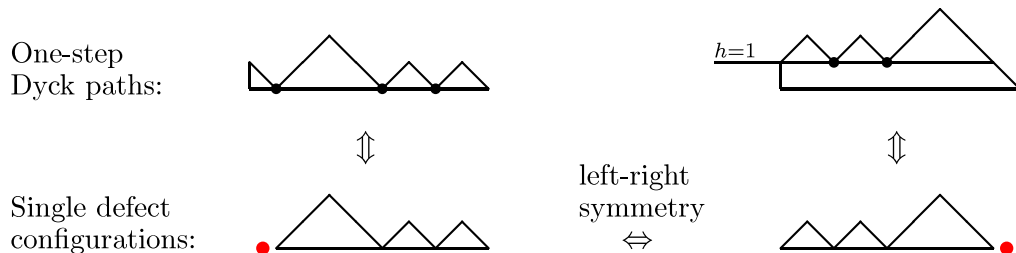
where $P_{L+1}(k, h_1 = 0(2))$ are stationary probabilities to find k clusters and the height $h_1 = 0(2)$ in the first site for the RPM with the odd number of sites $(L + 1)$:

$$P_{L+1}(k, h_1 = 0) + P_{L+1}(k, h_1 = 2) = P_{L+1}(k).$$

The first term in the sum (8.10) is a stationary contribution of the profiles with $(k - 1)$ return points at height $h = 0$ ($\Leftrightarrow n = L/2$, see figure 17) which is given by the conjecture:

$$P_{L+1}(k) = \frac{1}{S(L+1)} P\left(L+1, \frac{L}{2}, k-1\right). \tag{8.11}$$

To calculate the last two terms in the sum (8.10) we take into account the left-right symmetry of the one-defect profiles in the ‘defects’ picture of the one-step Dyck paths (see the appendix). As it is seen on the following picture



in the RPM of the odd size $(L + 1)$ the stationary weights of profiles with $(k - 1)$ contact points (i.e. with k clusters), one of them is at site 1 ($h_1 = 0$), are equal to the stationary weights of profiles with no contact points, but with $(k - 2)$ return points at height $h = 1$ ($\Leftrightarrow n = \frac{L}{2} - 1$, see figure 17). Therefore

$$P_{L+1}(k, h_1 = 0) = \frac{1}{S(L+1)} P\left(L+1, \frac{L}{2} - 1, k-2\right). \tag{8.12}$$

From (8.10)–(8.12) we obtain for L even

$$P_L^{(1)}(k) = \frac{1}{S(L+1)} \left\{ P\left(L+1, \frac{L}{2}, k-1\right) - P\left(L+1, \frac{L}{2} - 1, k-2\right) \right. \\ \left. + P\left(L+1, \frac{L}{2} - 1, k-1\right) \right\},$$

which is equivalent to (3.7) provided one takes into account the identity

$$P\left(L+1, \frac{L}{2}, m\right) - P\left(L+1, \frac{L}{2} - 1, m-1\right) = P\left(L+1, \frac{L}{2}, m+1\right)$$

for L even and $\forall m = 0, \dots, \frac{L}{2}$.

9. Conclusions

As far as we know the RPM with and without a wall is the only example of a one-dimensional fluctuating interface which is conformally invariant (the central charge of the Virasoro algebra $c = 0$ since in a stochastic process the ground state energy is zero for any system size). The time dependence of average quantities are under control since the finite-size scaling Hamiltonian spectrum is known (see [10, 16]). For space dependent phenomena, the situation is more complex since one does not know which critical exponents appear. What we do know is that, in the finite-size scaling limit, the functional dependence of density profiles in the stationary state are fixed once the scaling dimensions of the local operators and the boundary conditions are specified (see (4.3) and (4.5)). Our aim was to identify local operators by checking if the expressions (4.3) and (4.5) are confirmed by the data.

First we have considered the contact-point density profiles in the RPM and in the RPMW and found the density profiles in the finite-size scaling limit using Monte Carlo simulations. They have the expected behavior (see (4.3), (4.6) and (4.10)) for an operator with scaling dimension $X = 1/3$. This value is puzzling since as explained in section 4, it is incompatible with the Kac table for an operator of conformal spin zero (see (4.10)). The material presented in sections 6–8 in which one computes the probabilities to have k clusters ($k+1$ contact points) in the system gives a rigorous proof that the exponent is indeed $X = 1/3$. We would like to qualify what we mean by rigorous. The derivation is based on finding solutions of the split-hexagon recurrence relations (6.8) for the quantities $P(L, m, n)$. The identification of these quantities with certain Dyck path configurations as explained in section 7 remains a conjecture.

We have also considered the defect density profiles in the RPMW model and found the expected finite-size scaling function with an exponent $X = 1$ which is also puzzling since it is also incompatible with the Kac table for a spinless operator (see (4.16)). We have no rigorous proof that the exponent is 1 but the physics which follows (see (4.14)) is very plausible.

One easy way out of these puzzles is to bring the argument that in a $c = 0$ theory, everything is possible. We are tempted by another scenario: in both cases one has the conformal spin $s = X$. In this case both values $1/3$ and 1 are given by the Kac table but we run into a different problem: an operator with conformal spin has a vanishing density. Why this does not happen in our case, is another puzzle. Possibly there is a simple explanation, but it escaped us.

The model has many interesting properties as discussed in detail in section 4. One of them looks to us really unexpected: the connection between the clusters in the RPM and the parameter dependent (the boundary rate a) RPMW for an odd number of sites. Except for the first cluster, the two models are identical. The proof of this statement is in section 8. It is perhaps no accident that the function which gives the probability of

finding the first cluster at a distance x from the wall has special properties (see (4.18)). The implications of these observations on time dependent average quantities will be discussed elsewhere.

We would like to comment about the content of the mathematical part of this paper. Its relevance goes beyond finding a critical exponent and mapping of two models. In section 6 we give solutions for the so called Pascal's hexagon bilinear recurrence relations corresponding to certain boundary conditions. We also introduce new bilinear split-hexagon recurrence relations and solve them for certain boundary conditions. Their connection to integrable non-linear differential equations is still to be found.

Acknowledgments

We thank Jan de Gier, Vyacheslav Priezzhev, Philippe Ruelle and Alexander Zamolodchikov for valuable discussions and comments.

The work of PP and VR was supported by the DFG-RFBR grant (436 RUS 113/909/0-1(R) and 07-02-91561-a) and by a grant of the Heisenberg–Landau program. The work of PP was partially supported by the RFBR grant No 05-01-01086-a. The work of FCA was partially supported by FAPESP and CNPq (Brazilian Agencies).

Appendix. The RPM as a pair annihilation process with a source

In section 2 we have shown that the one-step configurations can be mapped onto configurations with one defect and clusters (see figures 2 and 3) and that the ballot path configurations can be mapped onto defect configurations. In a defect configuration, clusters start and end on sites and defects occupy links. We give some simple examples of the mapping.

In figure A.1 we show the three ballot paths for $L = 3$ and in figure A.2 we show the corresponding three defect configurations. The mapping is shown in figures A.3 and A.4 for $L = 4$. For a defect configuration with L even (odd), one has an even (odd) number of defects.

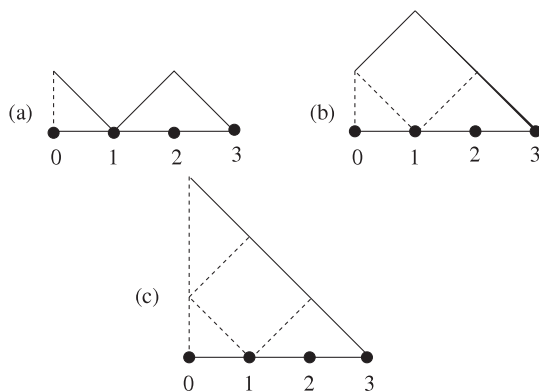


Figure A.1. The three ballot path configurations for $L = 3$ (four sites). In the stationary state of the RPMW all configurations are present while in the case of the RPM only configurations (a) and (b) (one-step Dyck paths) occur. The configurations should be compared with these of figure A.2.

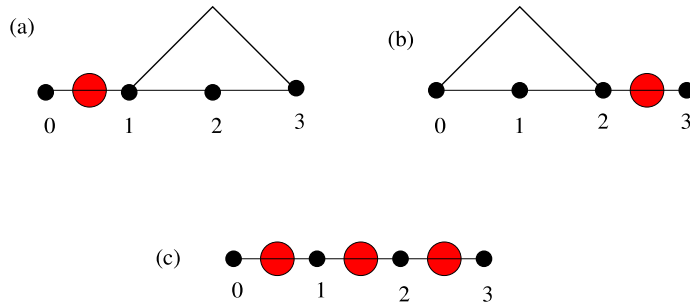


Figure A.2. The three configurations for $L = 3$ (four sites) formed by defects (red circles) and RSOS clusters. The corresponding ballot path configurations in the RPMW are given in figure A.1.

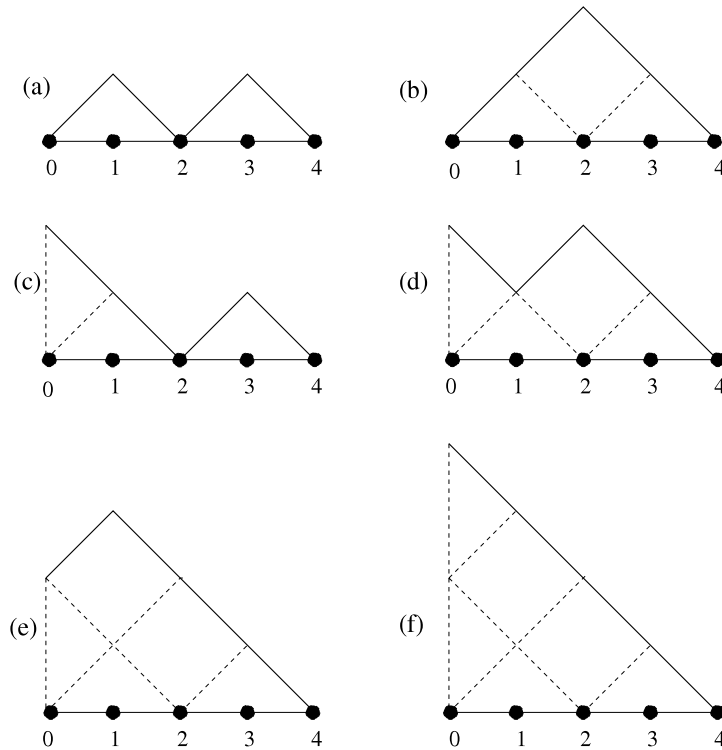


Figure A.3. The six ballot path configurations for $L = 4$ (five sites). In the stationary state of the RPMW all configurations are present while in the case of the RPM only configurations (a) and (b) occur. The configurations should be compared with these of figure A.4.

The dynamics of the RPMW, given in section 2 describing the evolution of the interface defined by ballot paths, can be translated in the evolution of the system defined by defect configurations. The evolution of the clusters is the same as in the RPM but the defects (impurities) hop over the adjacent clusters and in the hopping process they peel the clusters. When two adjacent defects annihilate they are replaced by a small cluster ‘building’ the substrate. The source acts non-locally: it adds a defect on the first site and another one at the end of the first cluster. We show now in detail the evolution process.

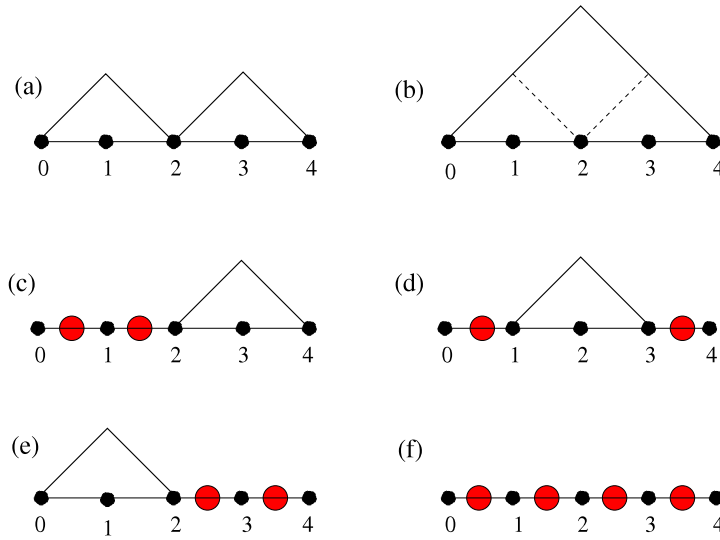


Figure A.4. The six configurations for $L = 4$ (five sites) formed by defects (red circles) and RSOS clusters. The corresponding ballot path configurations in the RPMW are given in figure A.3.

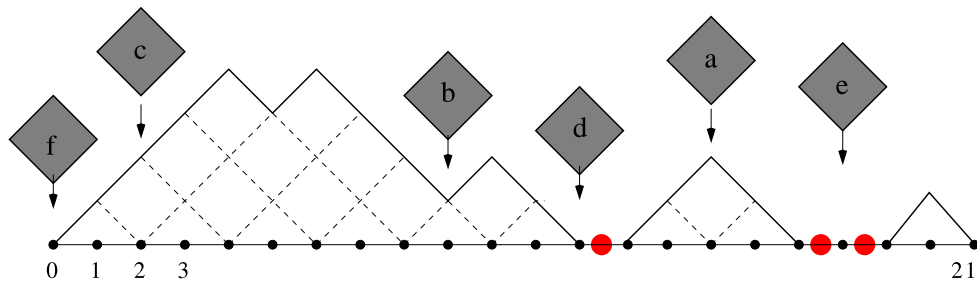


Figure A.5. One of the defect configurations for $L = 21$ (22 sites). There are three defects (red circles on the links) and three clusters. Also shown are six tiles (tilted squares) a-f belonging to the gas. When a tile hits the surface the effect is different in the six cases.

We consider a rarefied gas of tiles falling on a defect configuration with $L + 1$ sites. With a probability $p_b = 1/(L - 1 + a)$ a tile hits the bulk of the configuration (the sites $i = 1, \dots, L - 1$). With a probability $p_s = a/(L - 1 + a)$ a tile hits the boundary site $i = 0$. a is called the boundary rate.

The evolution rules depend on where the tile hits the configuration. In figure A.5 we show the different cases. In the cases a, b and c the tile hits a cluster and the rules are the same as in the RPM given in section 2. We give the rules for the cases d and e (see figure A.5).

- (d) The tile hits the site i which is at the right end of a cluster $h_j > h_{i-c} = h_i = 0$ ($j = i - c + 1, \dots, i - 1$). A defect is present on the link $(i, i + 1)$. The defect hops on the first left link of the cluster $(i - c, i - c + 1)$. In order to create a free link on which the defect hops, part of the outer layer is desorbed: if $h_{j+1} - h_j$ is

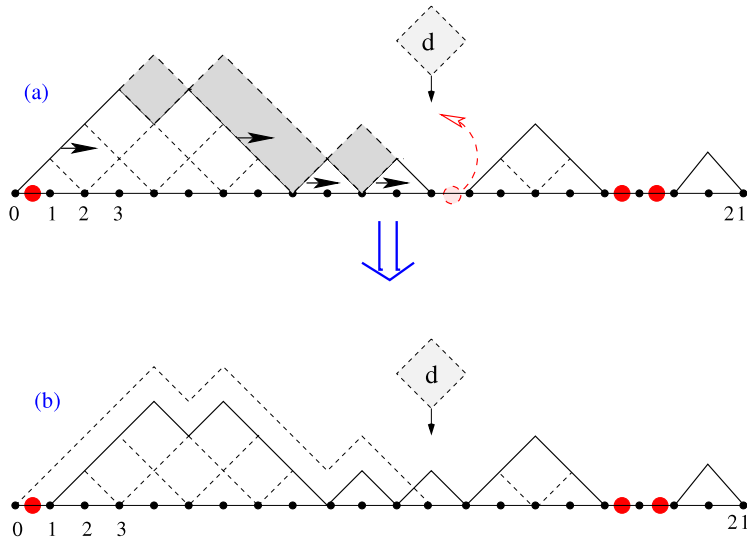


Figure A.6. The new profile after the tile *d* in figure A.5 has hit the surface at the right end of a cluster. The defect hops to the left end of the cluster, first peeling a layer of five tiles (a), and next, the peeled cluster is translated by a lattice spacing unit to the right (b).

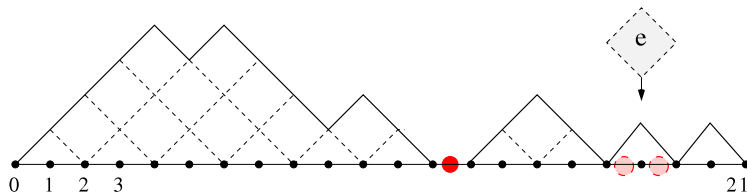


Figure A.7. The new profile after the tile *e* has hit the surface between two defects. The defects have disappeared and in their place one gets a new small cluster.

negative ($i - c + 1 \leq j \leq i - 2$) the tile, with the center at coordinates $(j, h_j - 1)$, evaporates (see figure A.6(a)), afterwards, the remaining cluster moves to the right by one lattice spacing ($h_j \rightarrow h_{j+1}$), as in figure A.6(b). An alternative way to visualize the process is shown in figure A.6(b). First a whole layer of the cluster evaporates $h_j \rightarrow h_j - 1$ ($j = i - c + 1, \dots, i - 1$). The defect hops from the link $(i, i + 1)$ to the link $(i - c, i - c + 1)$ and a half-tile cluster (part of the substrate) is created: $h_{i-1} = 0, h_i = 1, h_{i+1} = 0$.

- (e) The tile hits the site i between two adjacent defects placed on the links $(i - 1, i)$ and $(i, i + 1)$. The two defects annihilate and in their place appears a small cluster ($h_{i-1} = h_{i+1} = 0, h_i = 1$) (see figure A.7).

Up to now we have described the action of the RPM Hamiltonian H_L (see (5.10)) on the defect configurations. This model was used in [8] to study the pair annihilation process of defects in an unquenched disordered system. We now consider the effect of the boundary operator e_0 in the Hamiltonian $H_L^{(a)}$ (see (5.10)). This corresponds to the effect of a tile hitting the boundary site $i = 0$ (case f in figure A.5).

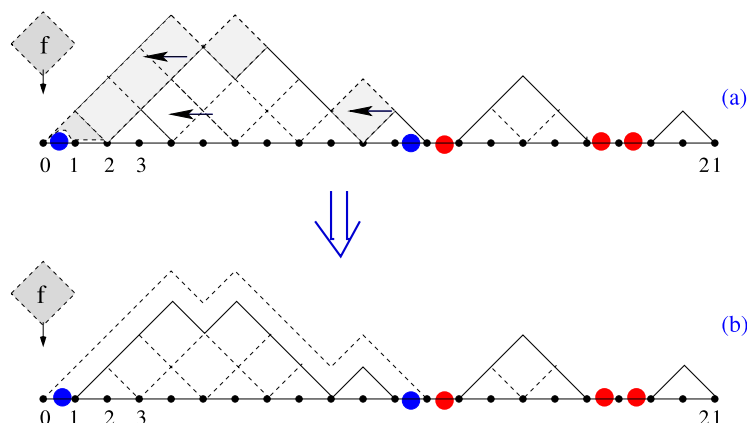


Figure A.8. The new profile obtained after a tile f in figure A.5 has hit the site $i = 0$ (the left side of a cluster defined by two contact points $h_0 = h_c = 0$, $c = 12$ in figure A.5). One first peels a layer of the cluster (5 tiles in the figure) (a), moves the remaining cluster by one unit lattice spacing to the left and then adds two defects (blue circles) (b). One on the link $(0, 1)$ and one on the link $(c - 1, c)$.

- (f) If the tile hits the site $i = 0$ and the link $(0, 1)$ is occupied by a defect, the tile is reflected. If there is no defect on the first link (this is the case f in figure A.5), the site $i = 0$ is the left end of a cluster $h_j > h_0 = h_c = 0$ ($j = 1, \dots, c - 1$) two defects are added to the configuration (one defect on the link $(0, 1)$ another one on the link $(c - 1, c)$) after peeling and moving the first cluster (see figure A.8(a)). If $h_{j+1} - h_j$ is positive ($0 \leq j \leq c - 3$) the outer tile, with center at coordinates $(j + 1, h_{j+1} - 1)$, evaporates, and the remaining cluster is moved to the left by one unit. An alternative way to visualize the effect of the tile which acts as a source of defects, is to first desorb a layer from the first cluster $h_j \rightarrow h_j - 1$ ($j = 1, \dots, c - 1$). Next the defects are introduced on the two links which became free as the result of the desorption process (see figure A.8(b)).

References

- [1] de Gier J, Nienhuis B, Pearce P A and Rittenberg V, *The raise and peel model of a fluctuating interface*, 2004 *J. Stat. Phys.* **114** 1 [[cond-mat/0301430](#)]
- [2] Alcaraz F C, Levine E and Rittenberg V, *Conformal invariance and its breaking in a stochastic model of a fluctuating interface*, 2006 *J. Stat. Mech.* **P08003** [[cond-mat/0604223](#)]
- [3] Alcaraz F C and Rittenberg V, *Different facets of the raise and peel model*, 2007 *J. Stat. Mech.* **P07009** [[cond-mat/0703725](#)]
- [4] de Gier J, *Loops, matchings and alternating-sign matrices*, 2005 *Discrete Math.* **298** 365 [[math.CO/0211285](#)]
- [5] Martin P P and Saleur H, 1994 *Lett. Math. Phys.* **30** 189
Martin P P and Saleur H, *The blob algebra and the periodic Temperley–Lieb algebra*, 1993 Preprint [hep-th/9302094](#)
- [6] Nichols A, Rittenberg V and de Gier J, *One-boundary Temperley–Lieb algebras in the XXZ and loop models*, 2005 *J. Stat. Mech.* **P05003** [[cond-mat/0411512](#)]
- [7] Shelton K, *The singled out game*, 2005 *Math. Mag.* **78** 15
- [8] Alcaraz F C and Rittenberg V, *The pair annihilation reaction $D + D \rightarrow 0$ in disordered media and conformal invariance*, 2007 *Phys. Rev. E* **75** 051110 [[cond-mat/0612272](#)]

- [9] Temperley H N V and Lieb E H, *Relations between percolation and colouring problems and other graph theoretical problems associated with regular planar lattices: some exact results for the percolation problem*, 1971 *Proc. R. Soc. A* **322** 251
- [10] Saleur H and Bauer M, *On some relations between local height probabilities and conformal invariance*, 1989 *Nucl. Phys. B* **320** 591
- [11] Razumov A V and Stroganov Yu G, *Spin chains and combinatorics*, 2001 *J. Phys. A: Math. Gen.* **34** 3185 [[math.CO/0012141](#)]
- [12] Razumov A V and Stroganov Yu G, *Combinatorial nature of ground state vector of $O(1)$ loop model*, 2004 *Theor. Math. Phys.* **138** 333 [[math.CO/0104216](#)]
- [13] Mitra S, Nienhuis B, de Gier J and Batchelor M T, *Exact expressions for correlations in the ground state of the dense $O(1)$ loop model*, 2004 *J. Stat. Mech.* P09010 [[cond-mat/0401245](#)]
- [14] Pyatov P, *Raise and peel models of fluctuating interfaces and combinatorics of Pascal's hexagon*, 2004 *J. Stat. Mech.* P09003 [[math-ph/0406025](#)]
- [15] de Gier J and Rittenberg V, *Refined Razumov–Stroganov conjectures for open boundaries*, 2004 *J. Stat. Mech.* P09009 [[math-ph/0408042](#)]
- [16] de Gier J, Nichols A, Pyatov P and Rittenberg V, *Magic in the spectra of the XXZ quantum chain with boundaries at $\Delta = 0$ and $\Delta = -1/2$* , 2005 *Nucl. Phys. B* **729** 387 [[hep-th/0505062](#)]
- [17] Bressoud D M, 1999 *Proofs and Confirmations. The Story of the Alternating Sign Matrix Conjecture* (Cambridge: Cambridge University Press)
- [18] Kuperberg G, *Symmetry classes of alternating-sign-matrices under one roof*, 2002 *Ann. Math.* **156** 835 [[math.CO/0008184](#)]
- [19] Robbins D P, *Symmetry classes of alternating sign matrices*, 2000 Preprint [math.CO/0008045](#)
- [20] Burkhardt T W and Xue T, *Density profiles in confined critical systems and conformal invariance*, 1991 *Phys. Rev. Lett.* **66** 895
Burkhardt T W and Xue T, 1991 *Nucl. Phys. B* **354** 653
- [21] Affleck I, *Edge magnetic field in the xxz spin- $\frac{1}{2}$ chain*, 1998 *J. Phys. A: Math. Gen.* **31** 2761
- [22] Cheng Z, Redner S and Leyvraz F, *Coagulation with a steady point monomer source*, 1989 *Phys. Rev. Lett.* **62** 2321
- [23] Hinrichsen H, Rittenberg V and Simon H, *Universality properties of the stationary states in the one-dimensional coagulation–diffusion model with external particle input*, 1997 *J. Stat. Phys.* **86** 1203 [[cond-mat/9606088](#)]
- [24] Batchelor M T, de Gier J and Nienhuis B, *The quantum symmetric XXZ chain at $\Delta = -1/2$, alternating sign matrices and plane partitions*, 2001 *J. Phys. A: Math. Gen.* **34** L265 [[cond-mat/0101385](#)]
- [25] Pearce P A, Rittenberg V, de Gier J and Nienhuis B, *Temperley–Lieb stochastic processes*, 2002 *J. Phys. A: Math. Gen.* **35** L661 [[math-ph/0209017](#)]
- [26] Date E, Jimbo M and Miwa T, *Method for generating discrete soliton equations III*, 1983 *J. Phys. Soc. Japan* **52** 388
- [27] Hirota R, *Discrete analogue of a generalized Toda equation*, 1981 *J. Phys. Soc. Japan* **50** 3785
- [28] Zabrodin A, *A survey of Hirota's difference equations*, 1997 *Theor. Mat. Fiz.* **113** 1347 [[solv-int/9704001](#)]
- [29] Speyer D E, *Perfect matchings and the octahedron recurrence*, 2007 *J. Algebr. Comb.* **25** 309 [[math.CO/0402452](#)]
- [30] Fomin S and Zelevinsky A, *The Laurent phenomenon*, 2002 *Adv. Appl. Math.* **28** 119 [[math.CO/0104241](#)]
- [31] Di Francesco P, *Inhomogeneous loop models with open boundaries*, 2005 *J. Phys. A: Math. Gen.* **38** 6091 [[math-ph/0504032](#)]
- [32] Zinn-Justin P, *Loop model with mixed boundary conditions, qKZ equation and alternating sign matrices*, 2007 *J. Stat. Mech.* P01007 [[math-ph/0610067](#)]